PDENG THESIS

Design of an Experimental Environment to Investigate Balance During Cycling and for Validation Purpose

ir. H. Kiewiet

Examination Committee
Prof. dr. ir. H.F.J.M. Koopman
Dr. ir. V.T. Meinders
Dr. ir. G.M. Bonnema
Dr. ir. R. Dubbeldam

Enschede, August 19, 2016

Table of Contents

Summary

The SOFIE project aims to improve the understanding of bicycle and rider stability in order to increase the safety of elderly cyclists. In the framework of this project, an advanced multi-body model of bicycle and rider dynamics, including the influences of the environment, is developed. The purpose of this model is to test, in the design phase, different concepts of so-called Intelligent Assist Devices in order to give direction to product design and development through mathematical modelling. It is therefore of high importance that results of this model are accurate. The experimental setup that is designed to validate the model is the main focus of the PDEng. In this setup a bicycle is instrumented with sensors to monitor dynamic behaviour of the rider and bicycle. Thereby determining the balance control strategy of the rider. In the setup the rear wheel of the instrumented bicycle rotates freely on a roller bench. The front wheel rotates on a treadmill to preserve the tire-road contact; steering can still be used to maintain balance. The roller bench is situated on a 6 degrees of freedom Stewart platform. The movement of the platform can be controlled in each direction. Therefore, it is possible to apply multiple disturbances to the bicycle with a predetermined multisine disturbance signal for identification purposes. Reference data is collected, in a save laboratory environment within controlled circumstances, to validate the mathematical model. Subsequently, it is possible to subject products, which enhance balance during cycling to controlled testing. Limitations of the used setup include loss of tire-road contact, possible visual distortion, exclusion of aerodynamic forces and the exclusion of studying cornering dynamics. However, the setup satisfies important requirements set in this study: the setup has provided an acceptable approach of the reality and allowed to accurately monitor the behaviour of the rider and bicycle.

Samenvatting

Het SOFIE-project doelt op het verbeteren van de stabiliteit van de fiets en fietser, om zodoende de veiligheid van oudere fietsers te verhogen. In het kader van dit onderzoek is er een multi-body model van fiets -en fietser dynamica ontwikkeld, waarin rekening wordt gehouden met invloed van de omgeving. Het doel van dit model is om gedurende de ontwerpfase verschillende zogenaamde ‘Intelligent Assist Devices’ te testen, om zo richting te kunnen geven aan het ontwerp en ontwikkeling van het product door middel van mathematisch modeleren. Het is daarom van cruciaal belang dat de resultaten van dit model accuraat, valide en betrouwbaar zijn. De opstelling die ontworpen is om het mathematisch model te valideren, is voornamelijk de focus van de PDEng. In deze opstelling is een fiets geïnstrumenteerd met verscheidene sensoren om het dynamisch gedrag te monitoren van zowel de fiets als fietser. Zodoende kan de balans strategie van de fietser bepaald worden. In deze opstelling roteert het achterwiel van de geïnstrumenteerde fiets vrij op een rollerbank. Het voorwiel roteert op een lopende band om zo het band-weg contact te behouden, sturen kan op deze manier nog steeds worden toegepast als balans strategie. De rollerbank is gelegen op een Stewart platform met 6 vrijheidsgraden. De beweging van dit platform kan daarom in elke richting worden aangestuurd. Zodoende is het mogelijk om meerdere verstoringen aan te bieden aan de fiets en fietser met een vooraf bepaalde multi-sinusoïde verstoringssignaal voor identificatie doeleinden. Referentie data wordt in gecontroleerde omstandigheden verzameld in een veilige laboratorium omgeving. Zodoende kan met deze referentie data het mathematisch model van fietsdynamica gevalideerd worden. Daarnaast is het mogelijk om balans-verhogende producten bloot te stellen aan gecontroleerde fietstesten. Limitaties van de gebruikte opstelling zijn verlies van het band-weg contact, mogelijke visuele verstoring, exclusie van aerodynamische krachten en de exclusie van bochtendynamica. Echter voldoet de opstelling aan belangrijke eisen, een acceptabele benadering van de realiteit is verkregen en de dynamica van het systeem kan accuraat gemonitord worden.

1. General Introduction

Cycling improves the health, mobility and the general quality of life, furthermore bicycling is an effective means of transportation. It is therefore in the benefit of society that bicycling should be available for people for as long as possible. The uptake of the electric bicycles in the recent years contributed to the mobility and social wishes and activities of elderly people. Especially where the health and strength reduces the cycling abilities of elderly people. However, an increasing number of people are facing a heightened feeling of insecurity on their bicycles as a result of an increasing number of elderly people are using cycling as a means of transportation or recreation. Decreasing motor –and cognitive skills (e.g. reaction time and hearing) can lead to more unexpected and dangerous traffic situations.

Factors as the sense of balance, getting on and off the bicycle and misjudgment of cornering and speed may lead to increased levels of danger. Secondly elderly people often have a decreased ability of multi-tasking during cycling, causing to hazardous situation. All these combined factors involving elderly people, have a consequence that at a certain point people stop riding their bicycles, simply because they are afraid. This has a big impact on their general health, since they are lacking the exercise. Subsequently, accelerating their decline in mobility and possibly health in general.

The current solutions for people who have problems balancing and riding their bicycles, is the change to a tricycle or a mobility scooter. This change is not easily made, because of the stigmatic character of these products and reduced mobility can be a result. Thus, room for improvement is found to increase the sense of safety and stability for elderly cyclists. To increase and improve the understanding of bicycle and rider stability, the SOFIE project is founded. SOFIE is an Dutch acronym for Slimme Ondersteunende Fiets (English: Intelligent assistive bicycle). The goal of the SOFIE-project is to develop intelligent assistive devices for electric bicycles to help elderly or cyclists with disabilities and to improve knowledge about bicycle stability especially with regards to elderly cyclists. The role of the Twente University in the SOFIE project is to provide knowledge on human balance control, the dynamics of the system of a bicycle, bicycle rider and their interaction with the environment (for example tire-road interaction) and technical developments which can assist in the development of the products.

1.1. Design Assignment

In the framework of this project, an advanced multi-body model of bicycle and rider dynamics, including the influences of the environment, is developed. The purpose of this model is to test, in the design phase, different concepts of so-called Intelligent Assist Devices In order to give direction to product design and development through mathematical modelling; it is of high importance that results of this model are accurate.

The research question formulated for this study is therefore: *"How can we collect reference data in a safe environment within controlled circumstances to measure dynamics of a rider and bicycle to validate an advanced multi-body model of bicycle and rider dynamics"*

The experimental setup that is designed to validate the model is the main focus of the PDEng. In the design, a bicycle is instrumented with sensors to monitor dynamic behavior of the rider and bicycle. Thereby, the balance control strategy of the rider can be determined. In the setup (see Figure 1) the rear wheel of the instrumented bicycle rotates freely on a roller bench. The front wheel rotates on a treadmill to preserve the tire-road contact; steering can still be used to maintain balance. The roller

bench is situated on a 6 degrees of freedom Stewart platform. The movement of the platform can be controlled in each direction. Therefore, it is possible to apply consistent, multiple disturbances to the bicycle with a predetermined multisine disturbance signal for identification purposes. Reference data is collected, in a safe laboratory environment within controlled circumstances, to validate the mathematical model. Subsequently, it is possible to subject products which enhance balance during cycling to controlled testing.

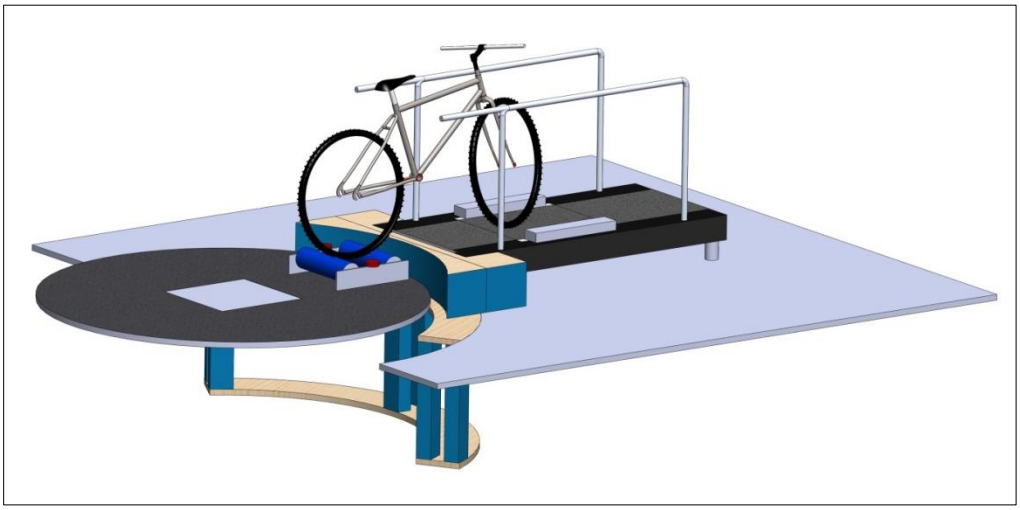

Figure 1, S*olid Works model of the design. Instrumented bicycle and infrared cameras are not included. Systems showed are the motion platform, treadmill, mounting accessory and safety.*

1.2. The SOFIE-Project

In this chapter the SOFIE projects is discussed more extensively. The structure and collaboration of the project is discussed. In that way a better understanding of the expectations within the project is obtained.

1.2.1 Project Structure

Multiple project partners were initially added to the SOFIE project to have a multidisciplinary team: marketing parties, knowledge generators and clinical parties, see Figure 2. In which each party has his own goals and deliverables and artifacts. Together, all generated knowledge and deliverables converge to the design and development of intelligent assistance devices (IAD's). Some artifacts are intrinsic knowledge on physical differences between elderly and young cyclist, evaluating (dis)mounting behavior of the bicycle, performing dual tasks whilst cycling and cycling whilst being perturbed. The IAD's are designed and constructed by Indes, which is the design/marketing partner. Initial more partners were part of the SOFIE project (a.o. regional bicycle supplier), however they decided to withdraw from the project.

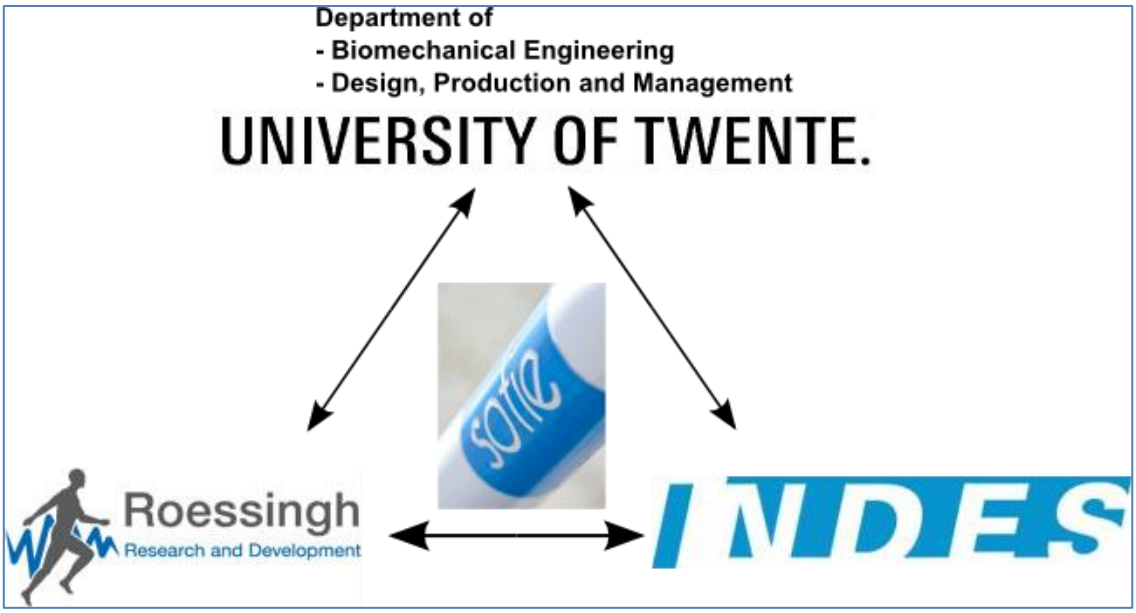

Figure 2, ***Structure of the SOFIE project.***

1.3. Design vs. Knowledge Problem

Two main research problems can be distinguished: design and knowledge problems. The two problems are related within a methodology framework, as is within the SOFIE project. The final goal for the SOFIE project is to design a bicycle that increases the stability of elderly cyclists, this can be geometric adaptation of the bicycle or (active) balance enhancing devices that can be implemented on the bicycle. The design of this more stable bicycle is a design problem.

The role of the PDEng assignment within the SOFIE project is to design an experimental setup, and performing and analyzing the actual measurements. However, there are two main goals of this setup. The first goal is to provide a validation dataset to validate an advanced multibody bicycle model the second goal is to generate knowledge on bicycle (active) stability. Both goals are achieved with the design of the experimental setup, see Figure 1. However both goals include a different problem. The investigation of bicycle stability is a research problem, whereas designing a setup to provide the validation dataset is a design problem (see Figure 3).

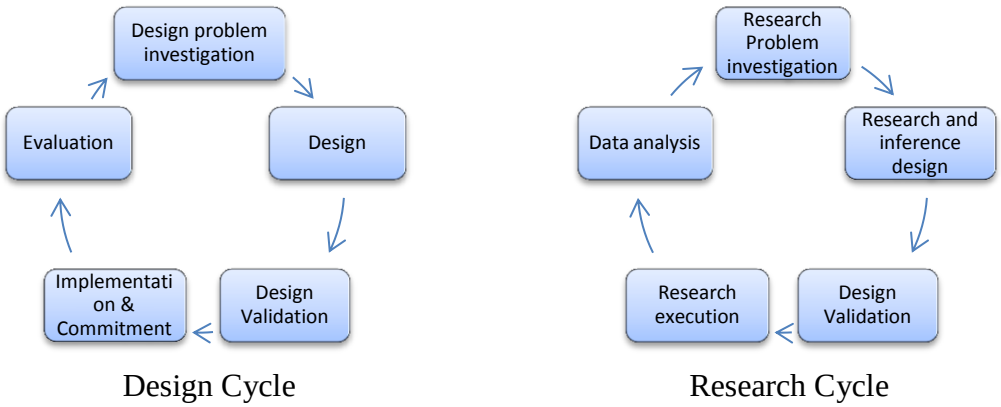

Figure 3, ***two main research problems and their respective cycle: Design and Research.***

2. Research Problem Investigation

Cycling is a very popular means of transportation in the Netherlands, and is gaining popularity in other prosperity countries. Next to an increasing health, bicycling for elderly causes independency and prevents social isolation. With the ageing population, more elderly cycle. However, ageing causes a decrease in physical fitness of elderly, creating difficulties for them to remain cycling. The recent uptake of the electrical bicycle ensures (physical challenged) elderly people to remain cycling at a higher age. However, two drawbacks of the electrical bicycle have come to daylight. The first obvious drawback is the high velocities that are easily reached with the electric bicycle. With a decreased physical strength and a decreased dual motor -and cognitive tasks performance, an increase single-sided accidents in complex traffic situations occurred. A second less obvious cause is the heavy weight of the electric bicycle. The bicycle is self-stable within a velocity frame. At velocities below the critical self-stability velocity, the cyclist must perform all the balancing tasks. The heavy electric bicycle increases the degree of difficulty to remain balanced below the critical self-stability velocity. Furthermore, often single-sided bicycle accidents with elderly cyclist using an electric bicycle take place during mounting –and dismounting the bicycle due to the increased weight of the electric bicycle.

To gain more knowledge on the behaviour of bicycles and balance strategies by cyclists, many studies have been performed using instrumented bicycles. Vlakveld et al performed field studies to study the speed choice and mental workload of elderly cyclists in complex traffic situations using two instrumented electrical assisted bicycles [1] In this study the each bicycle was equipped with a data storage unit in a box on the luggage carrier, a steering angle sensor, a tri-axis accelerometer, a rotation sensor in the bottom bracket, GPS and a speedometer. The velocity was measured with a dynamo embedded in the hub of the front wheel. Also subjects were equipped with sensors to measure physical parameters.

Cain et al performed field measurements to study steady state turning of a bicycle [2]. In this study the instrumented bicycle was equipped to measure angular velocity, acceleration and forward velocity of the bicycle. Furthermore steering angle and torque were measured. To measure the steering torque, a customized instrumented fork was used with an embedded torque sensor. An optical encoder to measure the steering angle.

Dubbeldam et al. performed field tests to investigate cycling strategies and mounting –and dismounting strategies of elderly cyclists. During this study subject and bicycle were equipped with XSENS inertial measurement units to measure the motion of each segment. Data was stored in a data storage unit in a box on the luggage carrier [3]. However, adding a storage unit directly to the bicycle has an impact on the inertia of the bicycle, and thus the intrinsic stability.

Kooijman et al studied normal bicycling to identify human control actions by measuring the vehicle motions and visual observation of the rider during field tests [4]. They instrumented the bicycle with a measurement computer on the rear back. Measured parameters were the steer angle and steer rate, rear frame lean –and yaw rate and forward velocity. The rates were measured using single axis angular rate sensors and the steering angle using a potentiometer. However, also collected data using a measuring computer seated on the rear rack.

Furthermore Kooijman et al also performed laboratory experiments [5]. During these experiments a large treadmill (3x5m) with regulated maximum speed of 25 km/h is used. The studied parameters were the same as during the field tests. Furthermore the studies the kinematics of the bicycle and rider using the Optrak Certus Motion Capture System.

Kooijman et al also performed studied cycling on a treadmill during perturbations to investigate how the human rider recovers from an unstable situation which was simulated by applying a lateral impulse to the rear frame [5]. During this perturbation the subject was not able to anticipate the lateral perturbations. The impulse was applied by a manually actuated rope tied to the seat tube. Manually introducing perturbation will result in a variation of added perturbations.

To study the vibrational comfort of the cyclist when cycling [6], Vanwalleghem et al. designed a custom-made contact force sensors based on strain gauges. Left –and right handlebar forces and saddle forces are measured, however two dimensional. Furthermore two accelerometers are placed at the saddle and both sides off the handlebar. Also pedal forces are measured using strain gauges placed on

the spindles. A crank encoder is used to determine the position of the crank. Data is wirelessly transmitted using Bluetooth transmission.
Many studies have focused on gaining knowledge on bicycle and rider behaviour; however to our knowledge no study has converted their finding to a product. Most studies are performed to gain knowledge on bicycle and/or rider stability [5, 7, 8]. The assignment of this PDEng is performed within the SOFIE project. The SOFIE project aims to improve the understanding of bicycle and rider stability in order to increase the safety of elderly cyclists. The final aim of the SOFIE project is smart assistive bicycle that directly improves the stability of the bicycle and rider. By conducting extensive research and thereby gain knowledge on understanding the important parameters influencing the intrinsic bicycle stability, an scientific foundation is created for the smart assistive bicycle.

3. Preliminary System Design

3.1. User Requirements

The aim of my assignment was to design an experimental setup to validate an advanced multi-body model of bicycle and rider dynamics, including the influences of the environment. The final deliverable was formulated as a controlled testing environment to determine the stability during cycling, including the necessary protocols. A number of requirements to which the design must hold are formulated. The main requirements of the system are as follows:

1) *The design should be an acceptable approximation of the reality.*
2) *The design should allow one to accurately monitor the behavior of the setup.*
3) *The design should be provided in a safe environment.*
4) *The design should allow controlled perturbations for identification purposes.*
5) *The design should allow to subject bicycles to products which enhance balance during cycling to controlled testing.*

Secondly a list of Sub Systems (artifacts) is constructed to schedule the separate functions and create an overview which systems are needed to properly validate the multi-body model and investigate bicycle dynamics in a controlled environment. A short overview of the final physical system is given in Appendix B. The following subsystems and there requirements are used for the setup:

- Instrumented bicycle;
-Measure Contact Forces between bicycle and rider.
-Able to measure front and rear wheel velocity.
-Able to measure Absolute steer angle.
- Safe environment;
-Presence of a safety harness
-Presence of a safety railing for grasping
-Presence of (an) emergency stop(s)
-Presence of a comfortable (dis)mount platform
- Kinematic tracking device;
-Able to measure dynamic behavior of bicycle and rider.
-Able to measure the above in different ways for synchronization purposes.
- Perturbation apparatus;
-Should be controllable
-Should be safe
- Experimental protocol;
-Must contain the necessary trials for identification purposes.
- Communication of sub-systems.
-No complex software tool should be used.
-Must not contain complex physical links

4. Design parameters

One of the requirements states that the design should allow one to accurately monitor the behaviour of the setup. This reason for this is that the output of the system should be used to validate the advanced multibody model of rider and bicycle. Therefore an accurate overview is necessary to determine which parameters are required to be measured.

4.1. Primary study parameters

The main study parameters of the kinematic study are the upper body -and lateral knee movement of the rider and steer angle of the bicycle. The upper body -and lateral knee movement of the rider and steer angle of the bicycle are used for stability evaluation during bicycle experiments. For the control identification experiments the primary study parameters are the control mechanisms the rider uses for controlling the bicycle: upper-body lean and lateral knee movement. With system identification techniques, the gains and time-delay of the controller can be identified.

4.2. Secondary parameters

The following kinematic parameters will be assessed. Additional kinematic parameters are the cycling velocity, which determines intrinsic bicycle stability, as well as the bicycle roll and yaw angle and their first and second derivatives. Furthermore, remaining human movement parameters are preferable measured, this includes postural dimensions such as segment lengths and pelvic width.

4.3. Other study parameters

Other additional parameters are the forces and torques on the pedals, handlebars and saddle, muscle activity of the arm muscles. The forces and torques at the contact points between the bicycle and rider provide more insight in the control mechanisms the rider uses to control the bicycle and can be used to better validate the computer simulation model.

The muscle activities of the arm muscles, measured by surface EMG, are a measure of the arm stiffness of the subject and are an important parameter of the computer simulation model as well.

Thirdly, for identification purposes, the rider and bicycle need to be disturbed. The motion or impulse of the perturbation is desirably measured as well.

4.4. Capturing Primary and Secondary parameters

To measure the aforementioned primary and secondary parameters, different methods can be applied: accelerometers such as XSENS, and motion tracking systems such as Visualize and Vicon. All systems have their advantages and disadvantages. In different studies within the SOFIE project, XSENS accelerometer in an inertia sensor attached to the frame of the bicycle and to the segments of the rider. The advantage of using these sensors is that they are wireless, easy to apply and allow field measurements outside. The disadvantage is that regularly contact with the receiver is lost, many sensors are necessary to accurately measure all kinematics and the time until the sensor is out of charge is short. The motion track system Visualize has the advantage that this system is mobile and requires little data processing afterwards. The disadvantage is that it is time-consuming to facilitate, underdeveloped software and easily disrupted calibration of the cameras. The advantage of the third system Vicon, is that the usability is convenient and that fixed infrared cameras are used. The disadvantage is time consuming data processing, it is not mobile and therefore it has a fixed environment. Both motion tracking systems have the tendency to lose the sensor out of sight from the camera which is inconvenient. All three movement tracker systems involve time-consuming preparation of the subjects. However, XSENS less time-consuming compared to other systems for

preparations of the subjects. The preparation of the subjects concerns adding (passive) markers to segments of bony landmarks of the subject. All systems require calibration sessions.

Apparently, for the primary and secondary parameters the use of which measurement system has both advantages and disadvantages. However, taking the additional parameters into account, one system distinguishes from other systems. The 3D motion tracking system Vicon allows one to measure both muscle activities with validated ‘of the shelf’ EMG sensors and applied forces with validated ‘of the shelf’ force –and torque sensors. Secondly, the 3D motion tracking system Vicon is installed in a laboratory setup, in which an 6 D.O.F. Stewart platform to allow external perturbations is embedded.

5. Measurement technologies and test procedures

In this chapter, a more extensive description of the used measurement setup and technologies are presented. Furthermore the protocol procedures of the experiments are elucidated. A complete overview of the final architecture of the systems is given in Appendix A to Appendix D.

5.1. Description of Experimental Setup

In the design a Trek L200 city bicycle with a straight handlebar is instrumented with sensors to monitor dynamic behavior of the rider and bicycle. Thereby, we can determine the balance control strategy of the rider. In the setup the rear wheel of the instrumented bicycle rotates freely on a roller bench. The front wheel rotates on a treadmill to preserve the tire-road contact; steering can still be used to maintain balance. The roller bench is situated on a 6 degrees of freedom Stewart platform. The movement of the platform can be controlled in each direction. Therefore, it is possible to apply multiple disturbances to the bicycle with a predetermined multisine disturbance signal for identification purposes. Reference data is collected, in a save laboratory environment within controlled circumstances, to validate the mathematical model. Subsequently, it is possible to subject products which enhance balance during cycling to controlled testing (see Figure 4).

Two measuring systems, a NI-USB 6218 data acquisition card (DAQ) and the marker-based Vicon motion capture system, are used to monitor the dynamics of the system. The system measures the kinematics of the bicycle, subject and Stewart platform, the contact forces between subject and bicycle (handlebars and saddle), rear -and front wheel velocity, pedal frequency and steering angle. The latter is measured with both systems, hence these signals are used for synchronization of the 2 measuring systems. Data stored via the DAQ is stored onto a laptop via 32 single ended channels, which stands nearby the treadmill on which the subjects is cycling. The DAQ has a power supply of max 10V and is CE marked. The DAQ is mounted on the rear end of the bicycle.

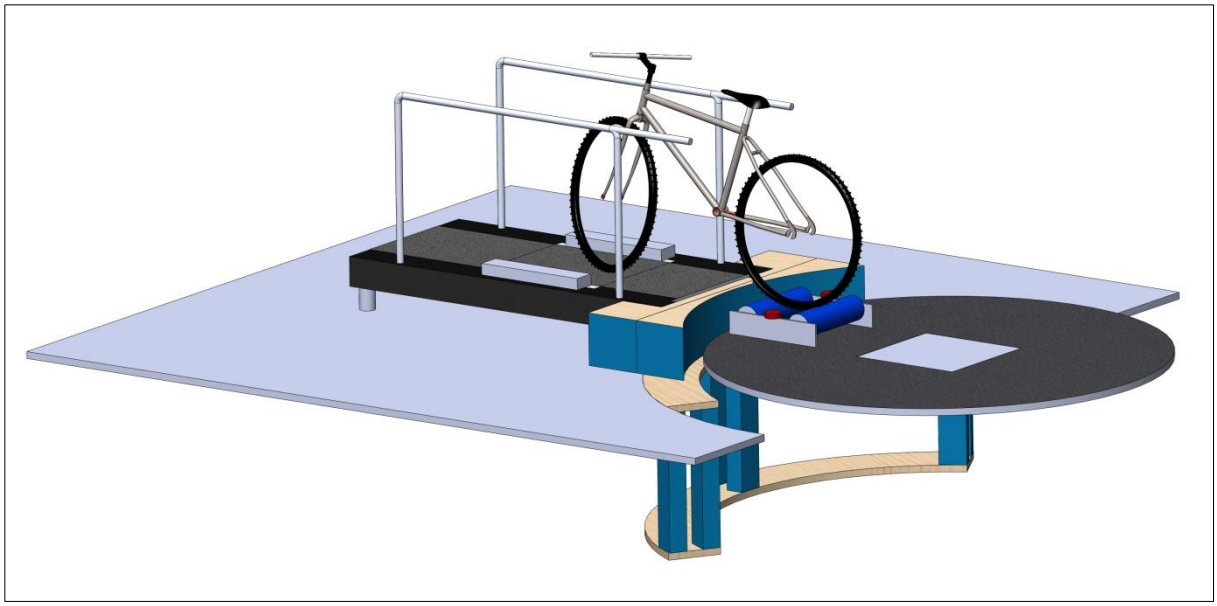

Figure 4, ***Solid Works model of the design. Instrumented bicycle and infrared cameras are not included. Systems shown are the motion platform, treadmill, mounting accessory and safety precautions.***

5.2. Measurement technologies

This paragraph consists of an extensive description of the used measurement systems. All used sensors are defined and the processing of data is described.

5.2.1. Motion Capture System VICON

This section described the features measured with the 3D motion capture system Vicon. Next to the kinematics of the bicycle and rider, also muscle activities and pedal forces are measured with Vicon.

5.2.1.1. Kinematics

3D Motion tracker Vicon is used to capture the kinematics of the bicycle and rider. Reflective markers were placed on bony landmarks to record 3D positions with the use of a motion capture system. The bony landmarks during cycling trials are defined as: the left -and right ulnar head, lateral humeral epicondyles, acromia, posterior superior iliac spine (psis), lateral femoral epicondyles and lateral malleoli, see figure Prior to the cycling trials, during a static stance trial, markers are also placed on the left and right anterior superior iliac spine (asis), medial femoral epicondyles, medial malleoli, calcanei and first metatarsal bone (Figure 5). A cluster of 3 markers is placed on the rear end of the bicycle to calculate the roll and pitch of the bicycle. A marker is placed on both ends of the handlebar for synchronization purposes with other measurement systems. Finally a marker is placed on both left and right pedal to accurately measure the pedal frequency.

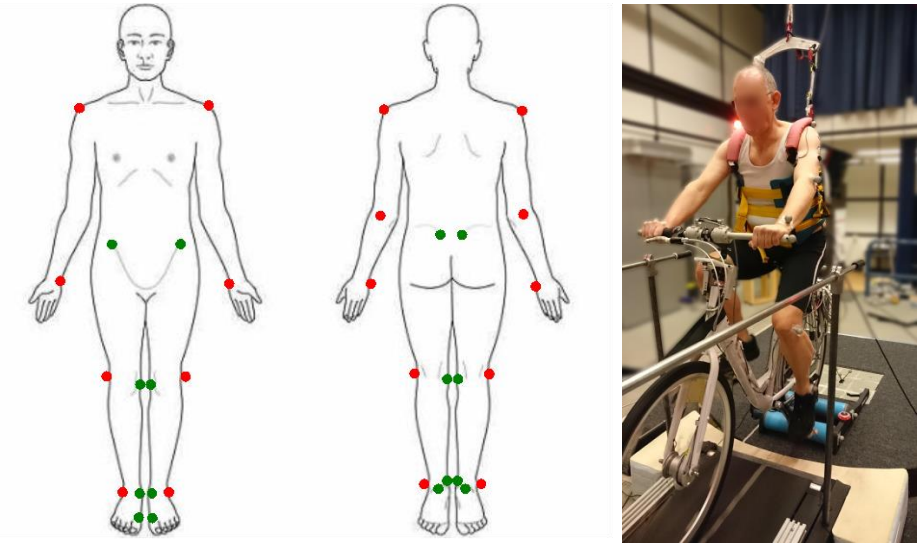

Figure 5, ***(right) Markers on the subject prior to the cycling trials (red and green) and during the cycling trials (red). (Left) example of old-adult subject during a cycling trials with visible reflective 3D at bony landmarks.***

5.2.1.2. Muscle Activity

The muscle activation of several left-hand side muscles have been measured during the cycling trials. The muscles and movements to which they primarily contribute, and therefore presumably during cycling tasks, are listed in Table 1. Maximal voluntary isometric contraction (MVIC) of the lateral triceps brachii and biceps brachii are captured to normalize their respective activations. EMG-Processing

Surface EMG (sEMG) signals are captured using 6 DE-2.1 EMG sensors and a BagnoliTM Delsys system and are amplified by 1kA. A reference node is placed on the C7 vertebra. Surface electrodes are placed on the muscles described in Table 1 according to Hermens et al. [9]. Figure 6 displays an

example of sensor placement. EMG is captured at 1560 Hz and down-sampled to 120 Hz. A second order Butterworth filter with cut-off frequency bandwidth of 10 to 60 Hz for the MVIC and 20 to 60 Hz for the cycling trials to adjust for movement artefact and noise. After applying the bandwidth filter, the signals are rectified. A smoothening moving average window of 0.25 seconds is applied to the signals. A low-pass filtered of 5Hz is applied to the biceps brachii and lateral triceps brachii signals during the cycling. The maximum found value for the MVIC is averaged over 100 ms, and is used to normalize the sEMG signals of respectively the biceps brachii and lateral triceps brachii.

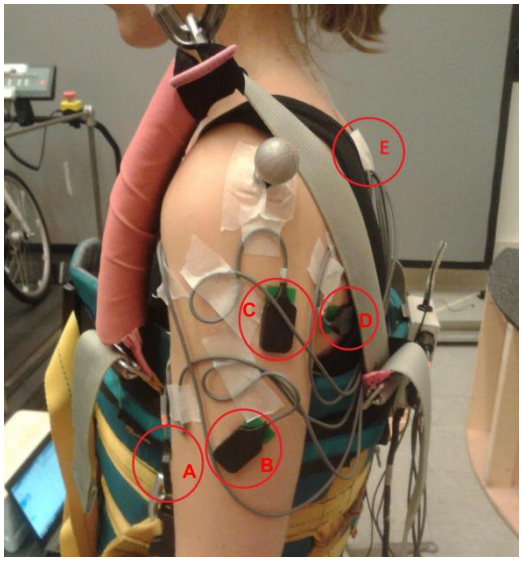

Figure 6, ***Example of the DE-2.1 EMG sensors located at the biceps brachii (A), lateral triceps brachii (B), posterior part of the deltoid (C) and the teres major (D). The pectoralis major and latissimus dorsi muscle are located underneath the safety harness and therefore not visible. A reference node is located at the C7 vertebra (E).***

Table 1

SELECTED MUSCLES

Muscle	Prime Involving Movement
Lateral Triceps Brachii	Elbow extension
Biceps Brachii	Elbow Flexion
Posterior Deltoid	Transverse extension of shoulder
Pectoralis Major	Flexion and adduction humerus
Latissimus Dorsi	Transverse extension etc
Teres Major	Transverse extension

Measured muscles during the experiments and the movements to which they primarily contribute during cycling tasks.

5.2.1.3. Pedal Forces

Since the setup is in a safe stationary environment, pedal contact forces can be obtained using wired force-torque sensors. Two ‘of the shelf’ multiaxial mini45 force-torque sensors are used. The calibrated ranges can be found in Table 2. These sensors are CE marked. The force-torque sensors are

each connected to the 3D Motion tracker system Vicon. Together with the raw-EMG signals, the output of the transducers is saved in a c3d construct for processing purposes. The calibrated ranges of the multiaxial mini45 force-torque sensors can be found in Table 2.

Table 2, ***calibrated ranges of the multiaxial mini45 force-torque sensors***

F_x	F_y	F_z	T_x	T_y	T_z
580 N	580 N	1160 N	20 Nm	20 Nm	20 Nm

5.2.2. Contact Forces

6 D.O.F. Force-Torque (FT) sensors are used to measure the contact forces between the bicycle and the cyclist. The FT sensors on the handlebar (left and right) and saddle tube are tailor made, pre-calibrated and contain integrated amplification (Sensix, Force-Torque Sensors). An ambulant external power supply is connected to the FT sensors. Output of each channel is collected via the DAQ. An A3 overview for the force sensors can be found in Appendix G.

5.2.2.1. Handlebar sensor

The handlebar sensors (Figure 7) are tailor-made by a French company Sensix. (http://www.sensix.fr/). The size of each handlebar sensor is 26mmx53mm. The weight of the sensors are 90g each, and are placed on the steer. Output voltage range is $\pm$10V. The electronic conditioning is integrated in the sensor. This sensor is CE marked. The calibrated ranges of the handlebar sensors can be found in Table 3

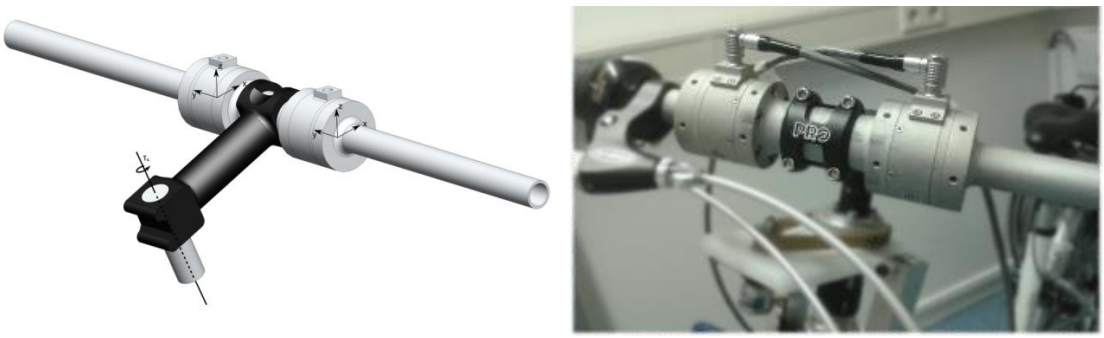

Figure 7, ***Left –and right handlebar force-torque sensor. Exerted handlebar forces and torques measured in the coordinate reference frames are used to calculate the exerted steering torque.***

5.2.2.2. Saddle tube sensor

The saddle tube sensor (Figure 8) is tailor-made by a French company Sensix. (http://www.sensix.fr/). The size of each handlebar sensor is 27mmx53mm. The weight is 180g and is placed on the saddle tube. Output voltage range is $\pm$10V. The electronic conditioning is integrated in the sensor. These sensors are CE marked. The calibrated ranges of the saddle tube sensor can be found in Table 3.

Figure 8, ***Saddle tube sensor on saddle tube. Superior on the tube sensor a mounting area for the saddle is present.***

Table 3, ***calibrated ranges of the multiaxial Sensix force-torque sensors***

Sensor	F_x	F_y	F_z	T_x	T_y	T_z
Handlebar	250 N	250 N	100 N	75 Nm	75 Nm	20 Nm
Saddle tube	500 N	500 N	1200 N	150 Nm	150 Nm	20 Nm

Both sensors use an external wireless power supply. Each sensor need a power supply of 4.5V-5V and 0.256 A. Therefore multiple 9V and 200 mA batteries are connected parallel. To reduce the 9V to the desired 5V, a 7805 regulator is used. The electrical circuit used for the external power supply for the force-torque sensors can be found in Figure 9. The output of the force-torque sensors are connected to the DAQ, as is the signal ground and the supply ground.

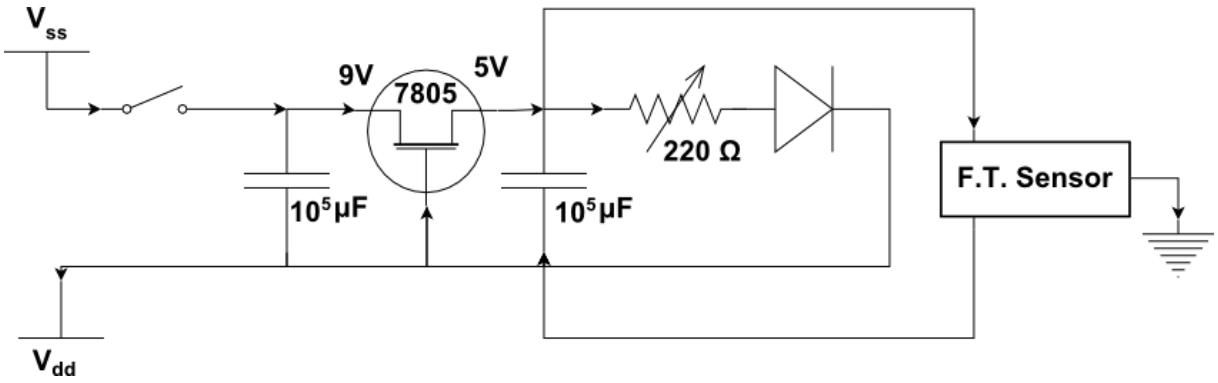

Figure 9, ***Electrical circuit for the external wireless power supply of the force-torque sensors. In this circuit 9V is transformed to the desired 5V. A switch is present for durability.***

5.2.3. Potentiometers

One potentiometers is mounted on the bicycle to measure the steering angle of the bicycle. A 360 degree servo potentiometer is mounted on the bicycle steer tube. The 360 servo potentiometer measures the absolute steering angle of the bicycle. Every measurement, the neutral potential value must be obtained to secure accurate steering angle values. The neutral potential value of the potentiometer indicated the voltage level at a steering angle of zero degrees.

5.2.4. Tilt Sensor

A 3g triple axis accelerometer (ADXL 335) is used to measure the tilt angles of the rear frame. This sensor is mainly used for 'back-up' data, if the 3D motion capture system Vicon fails to work. Supplied power is be between 1.8 and 3.6VDC. Dimensions are 18mmx18mm. The ADXL 335 is RoHS/WEEE lead-free compliant.

5.2.5. Hall Sensors

The velocity of the front and rear wheel is measured separately, both using a hall sensor and 9 magnets distributed equally on the wheel. A magnetic field sensitive switch is integrated in the hall sensor, allowing it to detect a neighboring magnetic field. To determine the optimal sampling frequency that ensures detecting a magnet by the hall sensor, Equation 1 is used. In which V is the velocity of the specific wheel, C is the circumference of the magnet distribution along the spokes, and circumference of the wheel, and D the diameter of one single magnet. The optimal sampling frequency is found to be 900 Hz. The pedal frequency is determined with two hall sensors, sensing two magnets placed distally on the left and right crank.

Equation 1 $$f_{optimal} = \frac{V_{wheel} \cdot C_{Magneting\ Ring}}{C_{Tire} \cdot D_{Magnet}}$$

5.2.6. Measurement Laptop

All data captured using the DAQ is stored at a measurement laptop via Matlab. The laptop is situated next to the treadmill. The measurement laptop is controlled using Teamviewer 10 from a remote laptop at a central control point. From this point 3 systems can be controlled: 3D motion capture system Vicon, the 6 d.o.f. Stewart platform and the measurement laptop.

5.2.7. Platform

In this session the front wheel of the instrumented bicycle is on a treadmill and the rear wheel rotates freely on a roller bench. The velocity of the treadmill is coupled with the velocity of the roller bench such that the velocity of the front and rear wheel are equal. The roller bench is situated at a six DOF steward platform (see Figure 4). The movement of the platform can be controlled in each direction and speed. Therefore, it is possible to apply disturbances to the roll, pitch and yaw and to apply lateral, posterior and superior disturbances to the bicycle with a predetermined disturbance signal. It is therefore possible to simulate disturbances which mimic real situations, e.g. side slip. Also combinations of different disturbances can be applied. The platform is controlled using 'Simulink'.

The perturbation signal used to control the platform, is a continuous multisine with 10 times a period of 10 seconds, sampled at 100 Hz, containing power at 10 frequencies: 0.4, 0.6, 0.8, 1.0, 1.2, 1.4, 1.8, 2.2, 2.6 and 3.0 Hz. Due to the multiple sinusoids, the signal is unpredictable for the cyclists, thus preventing anticipation of the perturbation. The signal has a descending power spectrum, containing more power at the low frequencies. The maximum amplitude was set to 1.75 cm for young subjects and 1.25 cm for the older subject group, to decrease the difficulty of the balance task.

5.2.8. Processing

All data captures is processed and analyzed using Matlab 2013a. The data is processed to a certain desired outcome parameters. These parameters are a.o. body segments movements in degrees, exerted forces in Newton and bicycle motion in degrees.

5.3. Experiments

In this section the conducted experiments are elaborated into more detail. Details of calibration trials, cycling trials are given.

5.3.1. Calibration

Calibration of the motion capturing system is needed to define the axes of rotation of the bicycle. The sensors on the bike are calibrated in two steps to determine the longitudinal axis and the tilt axis.

- The longitudinal axis is defined by rolling the bike from left to right with the steer 'fixed' 5 times in 3 sessions.
- The tilt axis is defined by rotating the bike at the steer 5 times in 3 sessions.

During these calibration measurements, the preloading of the force sensors is determined. Thereby determining the voltage output exerted by the force sensor without loading. Secondly, the voltage output is measured, with a passive rider. Indicating a rider mounted on the bicycle without cycling. During this calibration the bicycle is fixed within a static cycling test-bench.

5.3.2. Trials

30 subjects participated in this study. Two groups are distinguished: one group containing 15 healthy young subjects (25.3±2.8 yrs, 68.4±8.5 kg, 1.75±0.17 m) and one group containing 15 healthy older subjects (58.1±2.1 yrs, 75.8±7.7kg, 1.79±0.07 m). Saddle height is adjusted individually to the subjects' comfort. All subjects gave their written informed consent. The study was approved by the local medical ethical committee (Appendix H). The subjects were instructed to ride longitudinally on the treadmill without a predefined path. Since the front wheel velocity is driven by the treadmill and the rear wheel velocity by the subject, the subjects are imposed to a certain pedal frequency to ensure equal velocities of both wheels. The experiments were performed at different velocities: 7, 4, 3 and 2 m/s. The subjects are exposed to both 100s of unperturbed cycling and 100 s perturbed cycling. Table 4 shows the imposed pedal frequency and gear for each velocity of both subject groups.

Table 5 reflects the actual measured pedal frequency during both unperturbed and perturbed cycling.

The data is recorded with a sample frequency of 120 Hz. All data is pre-filtered with a second order Butterworth low pass filter with a cut-off frequency of 5 Hz. Thereafter the data was divided in two sections: unperturbed and perturbed cycling.

Table 4, ***overview of the imposed pedal frequency and gear for each velocity of both subject groups.***

Velocity (m/s)	**Imposed Pedal Frequency (Hz)**		**Imposed Gear (-)**	
-	Young Adult	Old Adult	Young Adult	Old Adult
7	0.97	-	7	-
6	-	0.97	-	6
4	0.87	0.87	4	4
3	0.77	-	2	-
2	0.68	-	1	-

Table 5, ***overview of the imposed and measured pedal frequency for each velocity of both subject groups.***

Group	Speed	Pedal frequency (Hz)	Actual Pedal frequency (Hz)	Difference
Young – Normal	**2**	0.683	0.720±0.060	+0.037
	3	0.767	0.783±0.026	+0.016
	4	0.867	0.887±0.033	+0.020
	7	0.967	0.960±0.074	-0.007
Young – Perturbation	**2**	0.683	0.726±0.060	+0.043
	3	0.767	0.794±0.037	+0.027
	4	0.867	0.899±0.053	+0.032
	7	0.967	0.988±0.037	+0.021
Elderly – Normal	**4**	0.867	0.931±0.068	+0.064
	6	0.967	0.965±0.071	+0.002
Elderly – Perturbation	**4**	0.867	0.934±0.071	+0.067
	6	0.967	1.004±0.049	+0.037

5.3.3. Perturbation

The perturbation signal was a continuous multisine signal of 100 s (10 times a repetition of a signal of 10 s) sampled at 100 Hz. The power was distributed over a limited number of frequencies, namely: 0.4, 0.6, 0.8, 1.0, 1.2, 1.4, 1.8, 2.2, 2.6 and 3.0 Hz (see Figure 10). Due to the multiple sinusoids, the signal was unpredictable for the cyclists, thus preventing anticipation of the perturbation. The signal had a descending power spectrum, containing more power at the low frequencies. The maximum amplitude was set to 1.75 cm for young subjects. Pilot testing revealed difficulties for the older subject group with this amplitude. Therefore, the maximum amplitude was set to 1.25 cm for the older subject group. The results were adjusted for the magnitude of the amplitude.

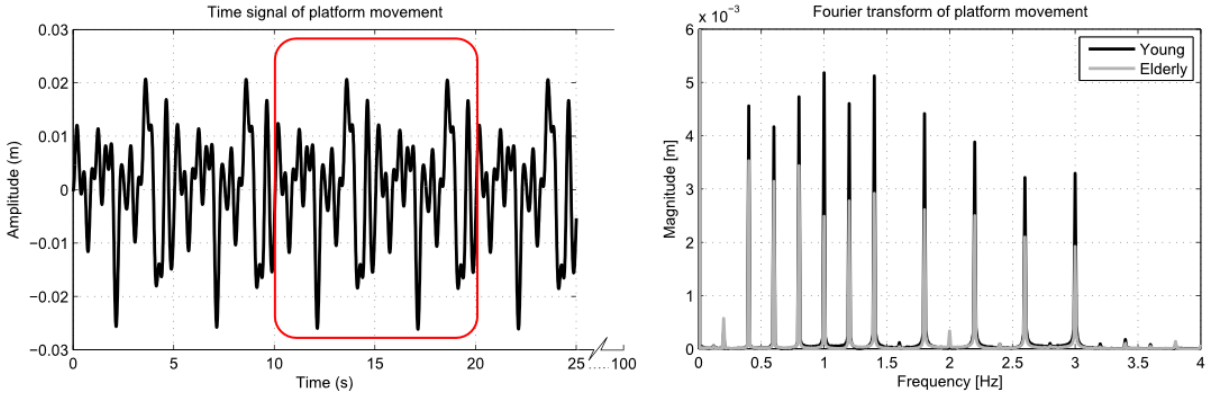

Figure 10, ***Representation of the continuous lateral platform perturbation. (a) Time signal of the platform movement. The perturbation signal is a continuous signal of 100 s (10 times a repetition of the same 10 s). (b) The Fourier transform of the platform movement, with power on 10 different frequencies and more power at low frequencies.***

6. Bicycle Parametrization

In this chapter the methodology to determine intrinsic bicycle parameters are described. A full set of parametrization is necessary to validate the advanced bicycle model. This parameter-set includes masses and inertias and center of masses of all bicycle segments: front –and rear wheel, rear frame and front assembly. Furthermore the wheelbase (wb), caster angle (λ), wheel radii ($r_{fw,rw}$) and trail (c) are determined (Figure 11).

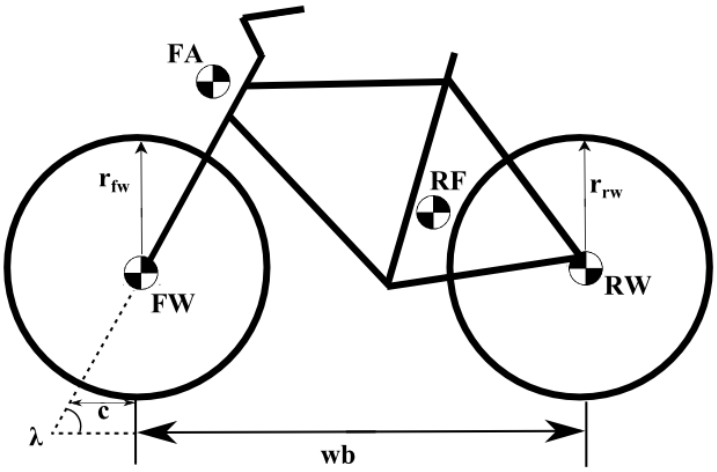

Figure 11, ***a schematic overview of a parametrization of the bicycle.***

6.1. Torsional pendulum

Inertia and the center of mass of the 4 segments (rear frame, front assembly, rear wheel and front wheel) are calculate using the method described by Moore et al [11].

A rigid fixture in constructed and mounted to a steel column. To the rigid fixture a titanium rod with a diameter of 4 millimeters is fixed. This rod is led through 2 ball bearings to reduce undesired pendulum motion. The ball bearings are assumed to be frictionless, wherefore no influence is exerted to the torsional motion of the titanium rod. A couple (Figure 12) is mounted to the end of the titanium rod to serve as a simple connection between the 4 segments and the titanium rod. The rate of oscillation was measured using an XSENS sensor at a sampling rate of 100 Hz. Each moment of Inertia measurement was performed 3 times. The function Equation 2 was fit to the raw resonance data using a fit type function in Matlab. Measurements are performed for 60 seconds after a small torsional perturbation is applied. The fit is applied to 33% to 66% of the raw resonance data to ensure torsional movement at resonance frequency.

Equation 2 $$\boldsymbol{A \cdot \sin(\omega_1 t + \varphi_1) + B \cdot \sin(\omega_2 t + \varphi_2) + C}$$

In which ω_1 represents the resonance frequency of the torsional motion.

6.1.1. Couple

The couple was calibrated using 3 different types of calibration units with known calculable inertias. Being a solid rigid a beam, a solid rigid cylinder and a hollow rigid cylinder. All calibration units are assumed to be homogenous. The inertia of the couple was determined and can be found in Table 6. These values should be used to correct the measured inertia values of the 4 segments.

Figure 12, ***used couple to serve as a connection between the titanium and the bicycle.***

Table 6, ***Inertia properties of the couple.***

Axis of Inertia	Inertia value
$\mathbf{I_x}$	0.0016 [kg m^2]
$\mathbf{I_y}$	0.0214 [kg m^2]
$\mathbf{I_z}$	0.0214 [kg m^2]

6.1.2. Measurements

After determining the inertia of the couple, the inertia and center of masses of all bicycle segments can be determined. The rear frame is mounted in 3 different configurations; see (Figure 13) an example of fit, using Equation 2, to obtain the resonance frequency is depicted in (Figure 14).

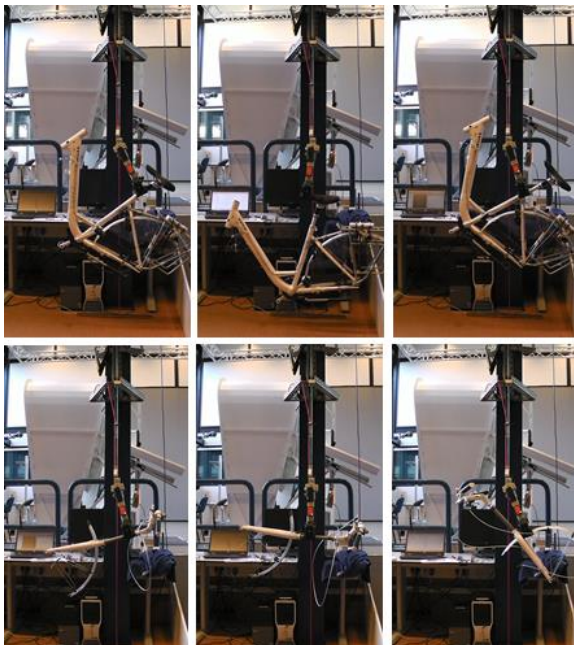

Figure 13, ***three different configurations of the rear frame (upper) and front assembly (lower) to determine the inertia and the center of mass of both segments.***

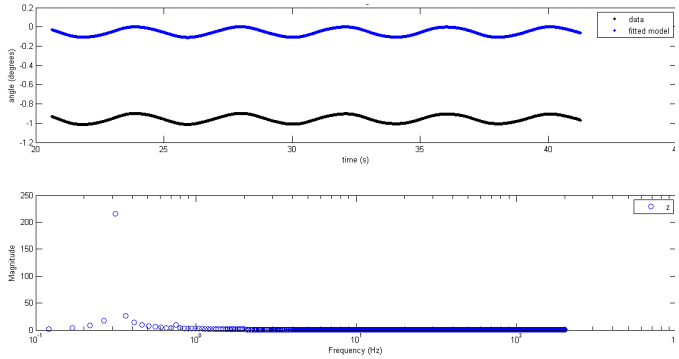

Figure 14, ***Example of a fit (blue) to the measured raw data (black) of the rear frame. An offset is added for graphical purposes (upper). A frequency analysis of the fitted function shows the resonance frequency of the rear frame. This frequency is used for calculating the inertia.***

The inertias then can be determined using Equation 3. In this equation, T is the period time and K the stiffness of the torsional rod. The stiffness can be calculated based on the shear modulus of titanium, and the length and the calculable inertia of the torsional pendulum.

Equation 3 $$\boldsymbol{Inertia = T \cdot K/(2\pi)^2}$$

To compensate for the Inertia of the couple, parallel axis theorem is applied (see Equation 4). With this theorem the mass moment of inertia of the rear frame can be determined.

Equation 4
$$\boldsymbol{I_{total} = I'_{couple} + m_c r_c^2 + I_{rear\ frame} + m_{rf} r_{rf}^2}$$
$$\boldsymbol{I'_{couple} = R \cdot I_{couple} \cdot R^T}$$

For each configuration the frame rotation angle β is calculated (Figure 15). This angle is defined as the rotation of the frame in the nominal configuration to the hanging orientation, rotated around the Y axis [11]. This frame rotation angle is used to recalculate the calculated inertia of the segment to the local reference frame.

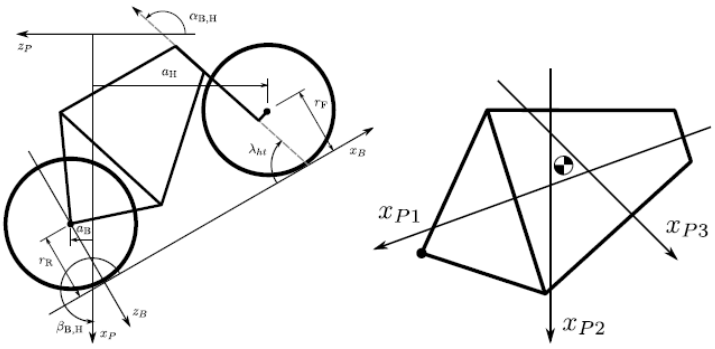

Figure 15, ***(left) description of the dimensions and angles that related the nominal bicycle reference frame with the pendulum reference frame. (Right) Exaggerated intersection of the three pendulum axed and the location of the center of mass.***

After calculating the inertia of each configuration for the rear frame and front assembly (Figure 13) and compensating for the inertia of the couple, the inertia of the rear frame can be calculated for the local reference frame of the bicycle (Figure 15), using Equation 5.

Equation 5

$$\begin{bmatrix} J_1 \\ J_2 \\ J_3 \end{bmatrix} = \begin{bmatrix} cos^2\beta_1 & -2sin\beta_1 cos\beta_1 & sin^2\beta_1 \\ cos^2\beta_2 & -2sin\beta_2 cos\beta_2 & sin^2\beta_2 \\ cos^2\beta_3 & -2sin\beta_3 cos\beta_3 & sin^2\beta_3 \end{bmatrix} \begin{bmatrix} I_{xx} \\ I_{xz} \\ I_{zz} \end{bmatrix}$$

A full set of measured torsional inertia's for each bicycle segment can be found in Appendix E.

6.2. Pendulum

After calculating the torsional inertias, the inertia around the lateral axis is determined. The inertia around the lateral axis is determined by measuring the period time after a pendulum perturbation. The front assembly is mounted to the front wheel, in which the hinge between the front wheel and front assembly is used as the pendulum. The same accounts for the rear frame and rear wheel (Figure 16). The inertia for each segment is calculated using Equation 6. In which m_r is the segments mass, g the gravity constant, l_r the pendulum length of the segment and l the total pendulum length.

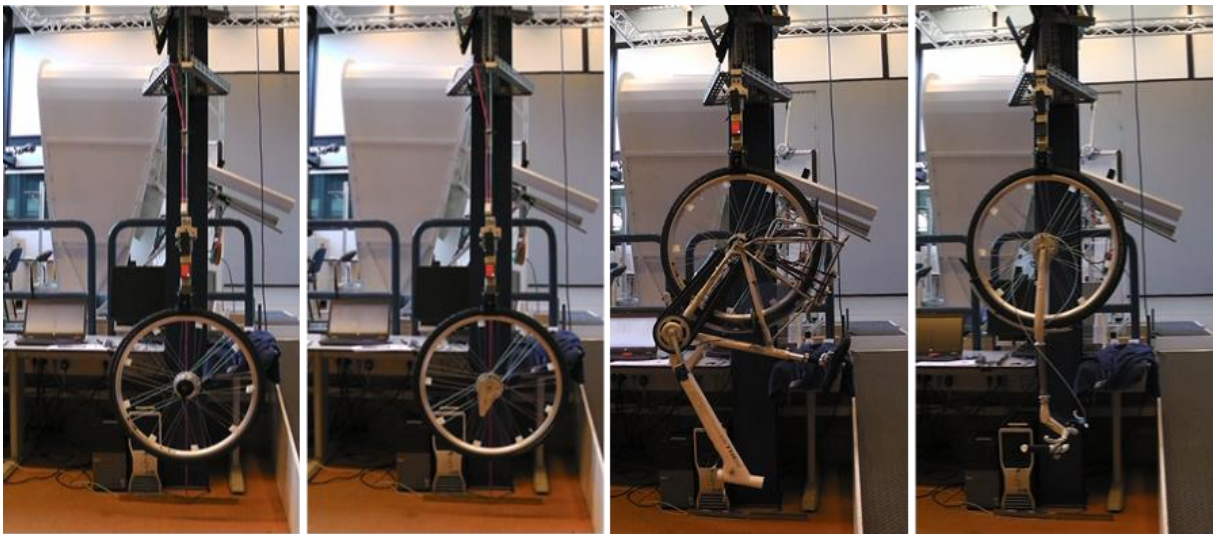

Figure 16, ***Pendulum configuration of respectively rear wheel, front wheel, rear frame and front assembly.***

Equation 6

$$I = \frac{T^2}{2\pi^2} m_r g l_r - m_r l^2$$

Finally, the calculated inertias are compensated for the inertia of the couple, and respectively the inertia of the rear wheel and front wheel for the rear frame and front assembly Equation 7

Equation 7

$$I_{y,rw} = I_{couple} + m_c r_c^2 + I_{y,rear\ wheel} + m_{rw} r_{rw}^2$$
$$I_{y,fw} = I_{couple} + m_c r_c^2 + I_{y,front\ wheel} + m_{fw} r_{fw}^2$$
$$I_{y,rf} = I_{couple} + m_c r_c^2 + I_{y,rear\ wheel} + m_{rw} r_{rw}^2 + I_{y,rear\ frame} + m_{rf} r_{rf}^2$$
$$I_{y,ff} = I_{couple} + m_c r_c^2 + I_{y,front\ wheel} + m_{fw} r_{fw}^2 + I_{y,front\ frame} + m_{ff} r_{ff}^2$$

The final calculated torsional and pendulum inertias of all bicycle segments: front –and rear wheel, rear frame and front assembly can be found in Appendix E.

6.3. Center of Masses

By choosing different configurations (Figure 13), the center of mass will line up always with the center of the longitudinal axis of the system. This longitudinal line is in fact a line in the nominal bicycle reference frame with a slope and a z-intercept (Figure 15). The slope and z-intercept can be calculated using Equation 8.

Equation 8

$$m_i = -tan\beta_i$$
$$b_i = -(\frac{a_B}{cos\beta_i} + r_R)$$

With this equation the final x and z coordinate can be determined using linear regression (Equation 9)

Equation 9

$$\begin{bmatrix} -m_1 & 1 \\ -m_1 & 1 \\ -m_1 & 1 \end{bmatrix} \begin{bmatrix} x_b \\ z_b \end{bmatrix} = \begin{bmatrix} b_1 \\ b_2 \\ b_3 \end{bmatrix}$$

Therefore, to determine the center of mass of the rear frame, the angle of the head tube, the distance of the rear axis to the middle and the distance of the couple's center of mass to the middle are measured for each configuration. The final calculated center of masses can be found in Appendix E.

7. Model comparison

In this section, the model to which the measured data set is applied for validation is introduced. Furthermore simulations of the model with an identical environment is performed and compared with modeled 'normal' cycling.

7.1. The model[12]

The mathematical model is developed in the commercial available multi-body dynamics software MSC ADAMS. The system of bicycle dynamics, rider biomechanics, rider control, a tire-road contact model and models of the environment are incorporated in one simulation environment. The bicycle dynamics are modelled with the use of four rigid bodies, similar to the frequently used 'Whipple' model [13]. The rider biomechanics are captured in 4 rigid bodies as well; the pelvis, the upper-body (containing the mass of the head, the trunk and the upper-arms) and both legs (Figure 1). Hence, certain rider movements are neglected.

The rider model contains five degrees of freedom: three rotational degrees of freedom of the upper-body with respect to the pelvis (a spherical joint, positioned at the L4-L5 vertebral joint) and one degree of freedom for both legs. The pedalling movement is initially neglected. Lateral knee movements are considered as a control mechanism at low speeds [14], and included in the model by a revolute joint allowing a rotation around the line connecting the hip and the ankle. The arms are modelled as linear spring-dampers (Ka) connecting the handlebars with the upper-body at the position of the shoulders, similar as in the motorcycle-rider model of Cossalter et al.[15]. The mass and inertia of the lower arms and the hands are added to the front fork.

The tire road contact is implemented using the PAC MC (Pacejka MotorCycle) tire model of the module Adams/Tire. This model is based on the Magic-Formula to fit experimental data of tires [16], that is currently considered as the state-of-the- art tire model for cars and motorcycles. Measurements on bicycle tires have been conducted at the University of Padova [17] and are used to determine the Magic Formula coefficients for the tire-road contact model.

Both the bicycle and rider model are fully parameterized, to enable modelling of any bicycle and rider. Furthermore, it allows parameter and optimization studies for improvement of the bicycle design (and possibly control). All parameters of the bicycle are measured using similar methods as Moore and Kooijman et al. [11]. The geometry and mass properties of the rider are estimated from the total weight and length of the person, using linear scaling and regression equations [18].

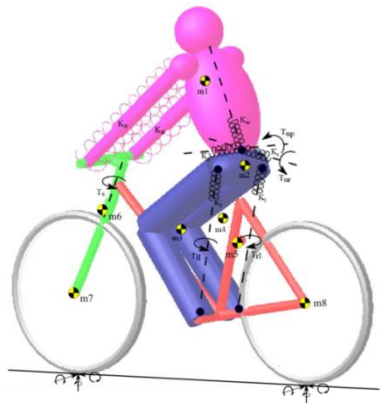

Figure 17, mathematical model of bicycle and rider constructed in MSC ADAMS.

7.2. Validation

The experiments are not only meant to provide insight into cycling dynamics and rider balance strategies, but also to provide a dataset for validation purposes. When the mathematical model is validated properly, this model can be used to study bicycle-rider dynamics, and subject the model to balance enhancing devices, or study the effect of intrinsic geometric adaptations of the bicycle. The

environment is therefore accurately modelled into the mathematical bicycle and rider model (see Figure 18). In this model, the Stewart platform copies the movement as during the measurement. The measured dynamics and forces are used as input for the model. The setup is modelled by sliding a road underneath the bicycle, causing the bicycle to have no global velocity. Via inverse dynamics internal forces can be predicted and compared. In the next paragraph an overview is provided how the internal forces acting by the body is calculated.

Figure 18, mathematical model of bicycle and rider with the roller bench, Stewart platform and treadmill included.

7.3.1 Calculating the Wrenches acting by the body

As a first step, all the local reference systems have to be defined for each segment. The origin of each reference system is located at the centre of each segment. Each segment is assumed to be cylindrical (see Figure 19). Passive markers are used to define the local coordinate systems its origin. The rotation from local to global, and the translation from the origin of the local to the origin of the local reference frame are then used to define the homogenous matrices.

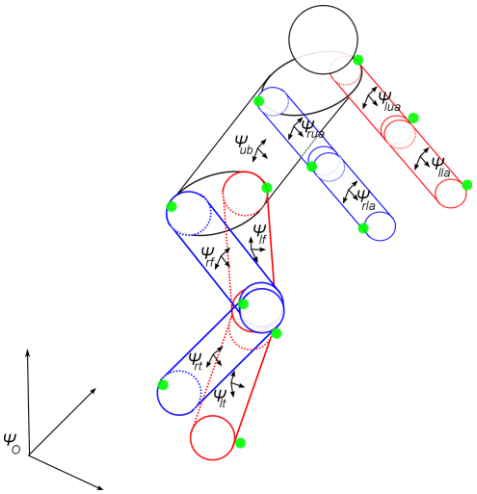

Figure 19, schematic overview of a rider without the bicycle. The rider is divided into several segments; each segment is assigned to a local reference frame. The green spots represent the passive markers used for kinematic tracking.

To eventually calculate the wrenches, thus the forces acting by the segments, we need to calculate the Twists of the moving segments. The twists can then be used to calculate the momenta of each segment. We consider the twist being defined as $\tilde{T}_i^{i,0} = H_0^i \cdot \dot{H}_i^0$, Thus the twist of Ψ_o expressed in the inertial frame Ψ_i. Note that $\dot{H}_i^0$ is the derivative of the inversed homogenous matrix H_0^i. Noise in

measurement data will be amplified due to derivation, therefore when applying derivation to measurement data a filter need to be applied to the dataset as well.

The calculated twists of the moving segments are used to calculate the momenta of the moving segments. For a point mass, the momenta is define as p=mv. This concept can be generalized to the defined segments using: $P^i = I^f \cdot T_i^{i,0}$. Where P^i is the momentum screw. The derivative of a momentum, results in a force: ${dp^o}/{dt} = F^o$. This can be generalized for the segments: $\dot{P}^i = W^i$.

Where $W^i$is the wrench, assemblage of the forces and torques acting by the segments.

Since the momenta are defined as $P^i = I^f \cdot T_i^{i,0}$, the derivative of the momenta is defined as: $\dot{P}^i = I^f \cdot \dot{T}_i^{i,0} + \dot{I}^f \cdot T_i^{i,0}$. In which I^f is Inertia tensor of the body segment. Containing the inertia around each axis, and the mass matrix. However the derivative of $\dot{I}^f = 0$ since this is a constant value. Therefore we can define: $\dot{P}^i = I^f \cdot \dot{T}_i^{i,0}$. Thereby using the aforementioned Twist of body i with respect to global reference frame, expressed in the local reference frame.

The derivative of the momentum screw can also be defined by Lie-Poisson reduction: $\dot{P}^i = ad^T_{T_i^{i,0}}(P^i) + W^i$. Which is the transpose of the adjoined matrix of the twist P^i. In which $ad_{T_i^{i,0}} = \begin{pmatrix} \widetilde{w}_i^{i,0} & 0 \\ \widetilde{v}_i^{i,0} & \widetilde{w}_i^{i,0} \end{pmatrix}$. Since we also have defined: $\dot{P}^i = I^f \cdot \dot{T}_i^{i,0}$, we can therefore construct the equation: $I^f \cdot \dot{T}_i^{i,0} = ad^T_{T_i^{i,0}}(P^i) + W^i$. Since it is the wrench, W^i that is desired. We can reformulate the equation to: $W^i = I^f \cdot \dot{T}_i^{i,0} - ad^T_{T_i^{i,0}}(P^i)$. Now we have an expression of the assemblage of the forces and torques acting by the segments in the local reference frame of each segment. Since we want to calculate the wrenches of each segment in the global reference frame, we have to apply a transformation to reference frame i via an adjunct matrix $Ad^T_{H_0^i}$. In which the adjoint representation can be written as $Ad_{H_0^i} = \begin{pmatrix} R_0^i & 0 \\ \tilde{p}_0^i R_0^i & R_0^i \end{pmatrix}$. Thus the calculation of the wrenches in the global reference frame can be written as: $W^0 = Ad^T_{H_0^i} \cdot W^i$. This calculation has been performed at each time frame for each segment: Left –and right tibia, left –and right femur and the HAT segment. Finally, all calculated wrenches can be summed for each time frame, resulting the total forces acting by the body during cycling: $W^0_{Body}(t) = W^0_{lt}(t) + W^0_{rt}(t) + W^0_{lf}(t) + W^0_{rf}(t) + W^0_{HAT}(t)$

The calculated wrenches, are the forces that the model should predict.

8. Risk Analysis

In Appendix F a risk analysis is found for the experimental setup. The risk analysis is roughly based on the hour glass method [19]. This method consists of 9 consecutive steps, being determining research domain, appointing final responsibility, describing main process and joined processes, forming expert team, determining critical events, risk factors and potential consequences, quantifying risks, determining preventive and severity reducing measures, assigning and detailing measures and finally reporting the findings. In the applied risk analysis, the steps determining research domain and appointing final responsibility, are not applied. A description of the main processes can be found in Figure 20.

Figure 20, main and joined processes cycling trial

The joined processes are Calibration of the measurement systems and verifying if they are functioning properly. Secondly familiarizing the subject with the setup, measurement equipment and protocols. Furthermore an adjoining process is preparing the subject by applying required sensors on the subjects using adhesives. Finally, closing down all measuring equipment and detaching sensors from subject if the measurement are completed.

The risk factor and potential consequences, quantification of these risks, preventive and quantification of the severity are summed up in Appendix F. The column reducing measures indicate which measures are taken to reduce the specific risk.

Table 7 contains an overview of all the determined preventive and severity reducing measures. The columns F and S represent the quantification of the frequency and severity. The original quantification of frequency and severity, suggested by the hourglass method et al. [19], are mainly focused on hospital cases. Therefore, the meaning of these quantifications has been adjusted slightly to the experimental setup. The indications for the quantification can be found in Table 8. The final column is the multiplication of the frequency and severity quantifications. These numbers represent the final risk quantification.

Table 7, *preventive and severity reducing measures.*

Prevention Measure	Description
1	Standardization of measurements with means of a protocol
2	Standardization of data storage
3	Adjusted protocol for old-adult subjects
4	Safety harness
5	Bumper wheels on roller bench
6	(Dis)Mounting accessory
7	Side Railing next to railing
8	Side Beams to prevent drifting of treadmill
9	Emergency stop for treadmill
10	Emergency stop for perturbation platform
11	Redundant rechargeable batteries
12	Recharge batteries in-between subjects
13	Periodical Upkeep in-between subjects
14	Daily periodical calibration of all systems
15	On -and off switch battery sensor
16	LED-light indicating on- and off state sensor
17	Metronome indicating pedal frequency
18	Supervisor for subject within range of emergency stop
19	Familiarization time for subject on setup
20	Remove excessive hair growth for EMG sensor
21	Apply alcohol before sensor adhesive
22	Breaks for subject in-between measurements
23	Redo measurement
24	Revise processing methods
25	Apply tape to reflecting noise

Table 8, *Indication of frequency and severity quantifications based on the Hour Glass Method.*

Quantification	Frequency (F) / Severity (S)	Indication
1	F	Every month
	S	Small
2	F	Every week
	S	Moderate
3	F	Every 2-3 measurements
	S	Reasonable
4	F	Every measurement
	S	Big
5	F	Every hour
	S	Catastrophic

As can be seen in the risk analysis (see Appendix F), the highest risks can be found concerning the subjects' safety. This is mainly due to the high accompanying severity. The safety of the subjects is

the most important concern of the design. As this was also one of the requirements: The design should be provided in a safe environment. It is therefore very important to secure the safety of the subject. However, most quantifications are in the ‘green-zone’, indicating that the experimental setup is safe to be exposed to intensive subject measurements. Only if al preventive and severity reducing measures are enforced. The most important preventive and severity reducing measures are the ones concerning directly the safety of the subject. These are an adjusted protocol for old-adult subjects, a safety harness, bumper wheels on roller bench, a (dis)mounting accessory, side railing next to railing, side beams to prevent drifting of treadmill, emergency stop for treadmill, emergency stop for perturbation platform, supervisor for subject within range of emergency stop and a familiarization time for subject on setup before the actual measurements. Most importantly, the local medical ethical committee has given a formal approval that the experimental setup is judged safe to perform the intended perturbation studies, see Appendix H for the original approval.

9. Design Validation

The roll of the Twente University is, amongst others, the design of an advanced multi-body model of bicycle and rider dynamics, including the influences of the environment. This model an effective and efficient manner to validate and evaluate IAD's, provided that the mathematical model is validated. The design a construction of a setup to investigate balance strategies during cycling serves therefore for validation purposes of the mathematical model as well. The experimental setup to validate the model was exposed to multiple trade-offs. For example, it was chosen to perform the experiments while cycling on a treadmill. This resulted in the loss of tire-road contact and external dynamic forces. However, safety measures could therefore easily be taken, and commercial of the shelf was used (e.g. motion capture systems).

The experimental setup is exposed to many pilot studies to determine if everything that is needed to be measured, is indeed measured, see Appendix A to Appendix D for a more extensive overview for the final architecture of the setup. This also means, that not only the data was measured properly, but also that the data was processed properly and convenient by means of Software tools as Matlab. A convenient way for structure processing of the data is with the tool model based system engineering (MBSE). The true value of MBSE is to improve the understanding of engineering disciplines within the project. It can facilitate and accelerates the system life cycle. The further in the life cycle, the more choices are details are known on specific sub systems. Relevant relations between concepts or components can be made. The increasing complexity can cause for a lack of understanding. By using model based system engineering order and overview can be created. Therefore it becomes more important the further a system design becomes. MBSE can therefore assist in managing large amount of datasets. In more systematics and detail, collateral understanding about how the data is managed and processed can be obtained, thereby saving time.

It is important that the perturbation applied to the system, are observed in the output of the system. The 'tweaking' of this perturbation deals with: amplitude, direction, frequency range and power spectrum trend. The one most important factor of the perturbation is that is should never endanger the safety of the subject. Therefore many pilot studies are used to finalize this perturbation. Perturbations are necessary for identification purposes of the model. Identification is a way to validate, and subsequently provides information on how elderly subjects react differently to unexpected perturbations than younger cyclists. This information can in turn aid in giving direction to accurate solutions to enhance the stability and safety of elderly cyclists by intervening where difference occur. Secondly, the validated bicycle model provided a very convenient way to enhance the self-stability range of a bicycle with means of a tool called design of experiments. With design of experiments, all parameters that define the bicycle can be changed (in) dependently to investigate their respective contribution to the self-stability of the bicycle. Thereby, we can create an optimized geometry of the bicycle. The geometry that provided the most optimized and realistic self-stable bicycle based on the tool design of experiments, led to the geometric adaptations of the final SOFIE bicycle, see Figure 21. Subjecting the revised bicycle to extensive experiments is necessary to finally assess the stability of this bicycle compared to stability of standard city bikes.

Figure 21, ***the final design of the SOFIE bicycle with geometric adaptation compared to a standard city bicycle resulting in a higher intrinsic bicycle.***

10. Discussion

10.1. Field perspective[12]

In this section the field perspective is discussed on the influences of forces acting on the dynamics of the bicycle.

Kooijman et al showed that bicycles are self-stable within a narrow speed range [5], this indicates that the rider is required to control the stability of the bicycle outside of these ranges. Not many studies have explored rider-induced stabilization in a controlled environment.

Cleary et al suggest that as a result of riding a bicycle on a roller bench, the role of the centrifugal force and a lack of inertia or forward momentum on rollers decreases stability of the bicycle [20]. Dressel et al however, make the counter-argument that even though a bicycle on rollers or a treadmill has no forward momentum in a frame of reference that is stationary with respect to the ground, it has the same balance dynamics (and thus stability) as the same bicycle on fixed surface [21]. This argument is based on the relativity, which states that the law of physics are the same in all inertial reference frames. We assume that this principle applies in the novel experimental setup we present in this paper, and proved with the use of a mathematical model. This implies however that the velocity and thus the pedal frequency during the experiments should be constant. In addition, it must be stated that the novel experimental setup does not allow the bicyclist to take corners. Nevertheless, we assume that if the path radius of the turning centre point is tracked, see Figure 22, a lateral acceleration is present of equal magnitude to the expression of the centripetal acceleration (Equation 10). The path radius of the turning centre point can be described based on the simplified equation for the kinematic steering angle, Δ, on flat level ground (Equation 11). From a geometric point of view, the kinematic steering angle is the angle of intersection between the road plane and the absolute steering angle [22].

Equation 10 $$a_c = \frac{1}{R} v^2$$

Equation 11 $$\frac{1}{R} \cong \frac{\tan \Delta}{p} = \frac{\cos \varepsilon \cdot \tan \delta}{p \cdot \cos \varphi}$$

In which R is the path radius of the turning centre point, v is the treadmill velocity, p is the wheelbase, φ is the camber angle of the rear wheel, ε is the caster angle, δ is the absolute steer angle and Δ is the kinematic steering angle.

Using these equations on the captured dataset of normal cycling shows that the lateral accelerations, if present, are indeed small. The mean of the maximal absolute calculated centripetal acceleration is 0.18 ms-2 ± 0.05 ms-2. Suggesting that little steering corrections while cycling on the novel apparatus are equal to corning with a large path radius, resulting in small lateral accelerations.

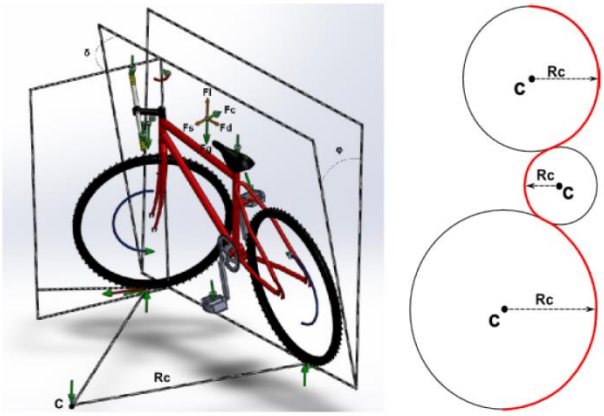

Figure 22, ***Overview of forces acting on the center of mass. Considering drag, lift, lateral, gravitational and centrifugal forces (Fd, Fl, Fs, Fg and Fc). Also the camber (φ) and steer (δ) angle are depicted. The right figure is an exaggerated display of the tracked path radius (Rc) of a centre point (C). The red line representing the travelled path of the bicycle.***

Cleary et al. state that the rider on rollers must stabilize the bicycle within a narrow path range [23]. Our findings however, show that large steering angles can easily be reached to stabilize the bicycle when the front wheel rotates on a treadmill. This suggests that the rider is comfortable in making large steering adjustments to maintain the stability of the bicycle, although bicycling within a narrow range, Figure 23.

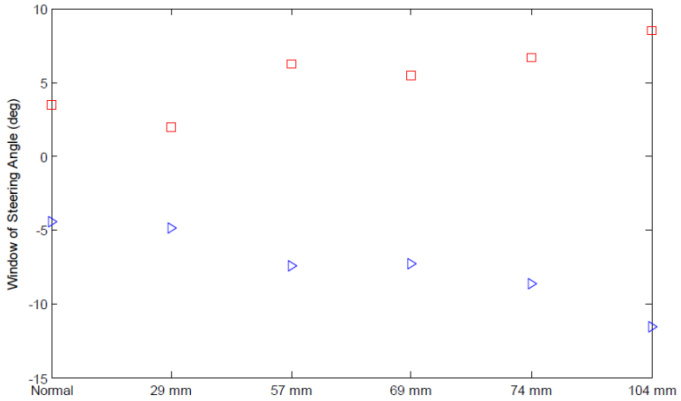

Figure 23, ***Window of steering angle of during a test trial of one subject depicting the maximum reached positive (red squares) and negative (blue triangles) steering angles for amplitude of lateral disturbance.***

The forces and moments acting on the tire-road contact are the longitudinal force, the lateral force, the vertical force, the overturning torque, the self-aligning -and twisting torque and the rolling resistance torque. Although the importance of these forces and torques to the steering dynamics have been proven in motor cycles [24, 25], it has not been demonstrated for bicycle steering dynamics. However, Doria et al have collected data of these forces and torques on bicycle tires [17], which have been introduced in the model describing the experimental setup. Results of the modelled experimental setup demonstrate the advantage of using the mathematical model to reproduce the dynamic behaviour of complex tire-road contact with the novel experimental setup.

10.2. Limitations

Certain limitations are present when cycling on a treadmill. These limitations involve cornering, visual distortion, tire-road contact and dynamic forces. These limitations are discussed in the following paragraphs.

10.2.1. Cornering

A very important part of cycling is cornering. Many studies have been conducted to investigate cornering of two wheeled vehicles [2, 22]. However, these involved steady-state cornering. Assuming steady-state simplifies the calculation of the dynamics of the two-wheeled vehicles. In the process of self-stability of bicycles, cornering is a very important aspect. To improve the stability of cycling, a fly-wheel has been proposed. This fly-wheel is an added gyroscopic effect to the front wheel of the bicycle. This concept is already available on the market, however is used as a training asset for children. The mechanics of the flywheel causes the bicycle to be very stable, thereby making it hard to fall over. However, due to dynamics of cycling, a roll angle is needed for the bicycle to initiate cornering. The flywheel making it therefore problematic for cornering.

During this study, with the used experimental setup, cornering was not studied. The main goal of the design was validation purposes of the mathematical model. Validation of this model did not require cornering. Although validating the mathematical model during (steady-state) cornering is eventually desired. Required for validation purposes of the controller was a multisine perturbation. Therefore cornering was not taken into account in the design.

10.2.2. Visual Distortion

A major point of discussion is the lack of movement of the surrounding environment. Cycling always involves translation of the environment from the riders reference centre. This effect is neglected whilst cycling stationary on a treadmill. The visual distortion can result in different or undesired behaviour of the subjects. Cain showed that cycling on a rollerbench is accompanied with a learning curve. However, during this study the tire-road contact of the front wheel deviated from standard tire-road contact due to the rollerbench [26].

However, more studies have been conducted involving bicycling on a treadmill [5, 8]. Though, the issue of visual distortion has not been addressed during this study. More research should be conducted to fully understand and comprehend the effect of this visual distortion on the riders' behaviour and dynamics. To ensure the learning curve as addressed by Cain et al. [26] and limit the effect of visual distortion, all riders were instructed to a 'learning' period. During this learning period, subjects are gradually subjected to cycling on the setup. This learning period was not time-bound, but lasted until the subject declares to be comfortable.

10.2.3. Tire-road contact

With the use of the previously described mathematical model, both situations are simulated. Allowing the difference between the two situations to be studied. When cycling on a treadmill, the road is always traveling in longitudinal direction of the treadmill. In a normal situation, without slide between the road and the wheel, the road is traveling in longitudinal direction of the front wheel. This difference can cause forces and moments to slightly differ in magnitude and direction and thus possibly slightly change the behaviour of the bicycle dynamics.

One factor which possibly influences the dynamics of a bicycle on a treadmill is an induced side-slip angle. The side-slip angle is the angle between the actual direction of travel of the wheel and the direction towards which it is pointing (Figure 24). Due to this side-slip angle a lateral force (F_y) at the contact patch is induced. The distribution of the lateral shear stress is asymmetric; therefor the resulting lateral force is applied at a point at a certain distance of the centre of the patch. This distance t, is called the pneumatic trail. From Figure 24 it can be seen that the lateral force generates a torque that tends to align the wheel at non-zero side-slip angles. This torque is therefore called the self-aligning torque and is a multiplication of the lateral force and the pneumatic trail. The self-aligning torque is a torque that tends to steer the tire toward the direction of travel and causes stability of the bicycle.

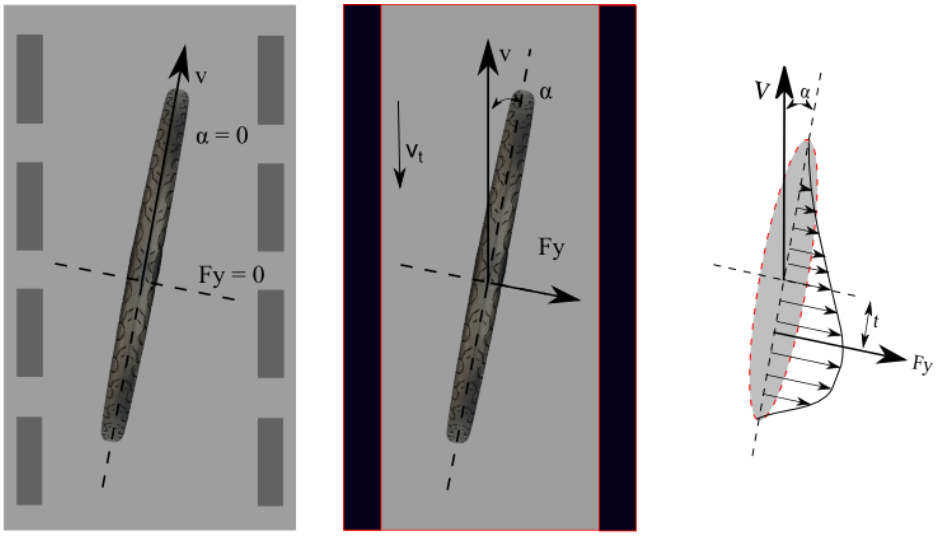

Figure 24, ***Front wheel with lateral force due to side-slip, for cycling on a road (left) and cycling on a treadmill (middle), and a depiction of the lateral shear stress profile in the contact patch (right). Note that no camber angle is present in this example.***

10.2.4. Dynamic forces

Because the rider-bicycle system has no forward velocity with respect to the world, certain forces do not apply to the system. These forces are the aerodynamic lift (Fl) and drag (Fd) force (Figure 22). Although lift force is of little influence on the system, the drag force is always actively present when cycling on the road [27, 28]. Fintelman et al state that the wind induced force is a function of the crosswind angle, in which the aerodynamic response has been recorded for a variety of crosswind angles. However, they also observed that the torso angle has little effect on the lateral force coefficient [28]. Bellolo et al suggests that the aerodynamic drag is about 80% of the total resistive force in road racing at 30 km/h. Velocities that during the experiments have been approached (ca. 25 km/hr). These conditions could have been approach using a wind tunnel. However, the absence of the frontal drag force on the bicycle dynamics is unknown. Though, this force is at all times in longitudinal direction of the bicycle. We therefore assume that this force has little to no role in the lateral balance. The lateral balance is investigated during this study. Limitations of the used setup include loss of tire-road contact, possible visual distortion, exclusion of aerodynamic forces and the exclusion of studying cornering dynamics. However, the setup satisfies the requirements set in the early stages of this study:

Conclusion

The aim of this study was to create a dataset for validation purposes of an advanced multi-body model of bicycle and rider dynamics. This dataset includes dynamics, kinematics and intrinsic properties of rider and bicycle. Data has been captured using a setup containing a bicycle instrumented with sensors to monitor dynamic behaviour of the rider and bicycle. Thereby determining the balance control strategy of the rider. In the setup the rear wheel of the instrumented bicycle rotates freely on a roller bench. The front wheel rotates on a treadmill to preserve the tire-road contact; steering can still be used to maintain balance. The roller bench is situated on a 6 degrees of freedom Stewart platform. The movement of the platform can be controlled in each direction. Therefore, it is possible to apply multiple disturbances to the bicycle with a predetermined multisine disturbance signal for identification purposes. Limitations of the used setup include loss of tire-road contact, possible visual distortion, exclusion of aerodynamic forces and the exclusion of studying cornering dynamics. However, the setup satisfies the requirements set in the early stages of this study: the setup has provided an acceptable approach of the reality, allowed to accurately monitor the behaviour of the rider and bicycle, is provided in a safe environment, allowed controlled perturbations for identification purposes and could allow to be subjected to controlled testing of balance enhancing products. Therefore we conclude that the used setup allowed us to collect reference data in a safe environment within controlled circumstances to measure dynamics of a rider and bicycle to validate an advanced multi-body model of bicycle and rider dynamics.

References

1. Vlakveld, W.P., et al., *Speed choice and mental workload of elderly cyclists on e-bikes in simple and complex traffic situations: A field experiment.* Accident Analysis & Prevention, 2015. **74**: p. 97-106.
2. Cain, S.M. and N.C. Perkins, *Comparison of experimental data to a model for bicycle steady-state turning.* Vehicle System Dynamics, 2012. **50**(8): p. 1341-1364.
3. Dubbeldam, R., et al., *The different ways to get on and off a bicycle for young and old.* Safety Science, 2016.
4. J.D.G. Kooijman, A.L.S., and J.K. Moore. *Some observations on human control of a bicycle*. in *ASME International Design Engineering Technical Conferences & Computers and Information in Engineering Conference,* . 2009. San Diego.
5. J. D. G. Kooijman, A.L.S. *Experimental validation of the lateral dynamics of a bicycle on a treadmill*. in *ASME International Design Engineering Technical Conferences & Computers and Information in Engineering Conference*. 2009. San Diego.
6. Vanwalleghem, J., et al., *Field tests with an instrumented bicycle for comfort measurements.* Journal of Science and Cycling; Vol 3, No 2 (2014): World Congress of Cycling Science 2014, 2/3 July 2014, Leeds, 2014.
7. Breitenecker, F., et al., *8th Vienna International Conferenceon Mathematical ModellingBicycle Rider Control Modelling for Path Tracking.* IFAC-PapersOnLine, 2015. **48**(1): p. 55-60.
8. Schwab, A.L., J.P. Meijaard, and J.D.G. Kooijman, *Lateral dynamics of a bicycle with a passive rider model: Stability and controllability.* Vehicle System Dynamics, 2012. **50**(8): p. 1209-1224.
9. Hermens, H.J., et al.,, *European Recommendations for SurfaceElectromyography; Results of the Seniam Project.*, 1999, Roessingh Research andDevelopment: Enschede.
10. Hermens, H.J., et al., *European Recommendations for Surface ElectroMyoGraphy; Results of the SENIAM project*. 1999, Enschede: Roessingh Research and Development.
11. Jason K. Moore, M.H.a.D.L.P., A. L. Schwab and J. D. G. Kooijman, *Accurate Measurement of Bicycle Physical Parameters*, in *Symposium on the Dynamics and Control of Single Track Vehicles*,2010: Delft, The Netherlands.
12. H. Kiewiet, V.E.B., D. van de Belt and H. F. J. M. Koopman. *A Novel Experimental Setup to Apply Controlled Disturbances to Bicycle Dynamics in a Safe Environment*. in *ASME 2014 International Design Engineering Technical Conferences and Computers and Information in Engineering Conference*. 2013. Buffalo.
13. Whipple, F.J.W., *The Stability of the Motion of a Bicycle.* The Quarterly Journal of Pure and Applied Mathematics, 1899. **30**: p. 312–348.
14. Moore, J.K., et al., *Rider motion identification during normal bicycling by means of principal component analysis.* Multibody System Dynamics, 2011. **25**(2): p. 225-244.
15. Cossalter, V., et al., *The effect of rider's passive steering impedance on motorcycle stability: Identification and analysis.* Meccanica, 2011. **46**(2): p. 279-292.
16. Pacejka, H.B., *Tire and Vehicle Dynamics*. Tire and Vehicle Dynamics. 2006.
17. Doria, A., et al., *Identification of the mechanical properties of bicycle tyres for modelling of bicycle dynamics.* Vehicle System Dynamics, 2013. **51**(3): p. 405-420.
18. Chandler, R., et al.,, *Investigation of inertial properties of the human body*, 1975, DTIC Document.
19. Dijk, Y.A.v., *Risicoanalyse methoden voor medische technologie : een vergelijking van de HMFEA en het zandlopermodel*, 2009.
20. Cleary, P.A. and P. Mohazzabi, *On the stability of a bicycle on rollers.* European Journal of Physics, 2011. **32**(5): p. 1293-1301.
21. Dressel, A. and J.M. Papadopoulos, *Comment on 'On the stability of a bicycle on rollers'.* European Journal of Physics, 2012. **33**(4): p. L21-L23.
22. Cossalter, V., R. Lot, and M. Massaro, *Motorcycle Dynamics*, in *Modelling, Simulation and Control of Two-Wheeled Vehicles*. 2014. p. 1-42.

23. Cleary, P.A. and P. Mohazzabi, *Reply to 'Comment on "on the stability of a bicycle on rollers"'*. European Journal of Physics, 2012. **33**(4): p. L25-L26.
24. Dressel, A. and A. Rahman, *Measuring sideslip and camber characteristics of bicycle tyres.* Vehicle System Dynamics, 2012. **50**(8): p. 1365-1378.
25. Plöchl, M., et al., *On the wobble mode of a bicycle.* Vehicle System Dynamics, 2012. **50**(3): p. 415-429.
26. Cain, S.M., D.A. Ulrich, and N.C. Perkins. *Using measured bicycle kinematics to quantify increased skill as a rider learns to ride a bicycle*. in *ASME 2012 5th Annual Dynamic Systems and Control Conference Joint with the JSME 2012 11th Motion and Vibration Conference, DSCC 2012-MOVIC 2012*. 2012.
27. Belloli, M., et al. *Handbike aerodynamics: Wind tunnel versus track tests*. in *Procedia Engineering*. 2014.
28. Fintelman, D.M., et al. *The effect of crosswinds on cyclists: An experimental study*. in *Procedia Engineering*. 2014.

Appendix A – System of Systems

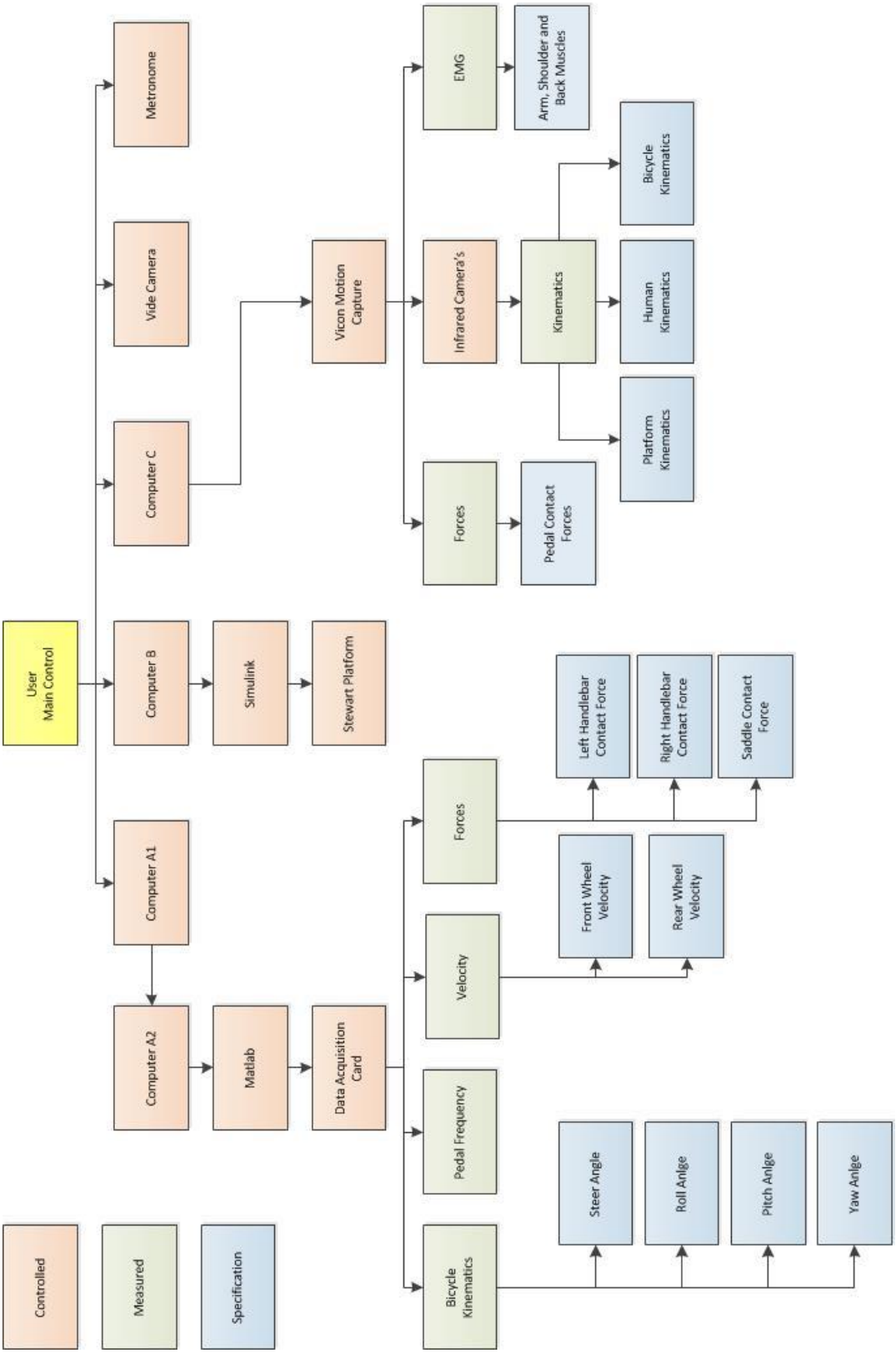

Appendix B – Schedule of Physical Systems

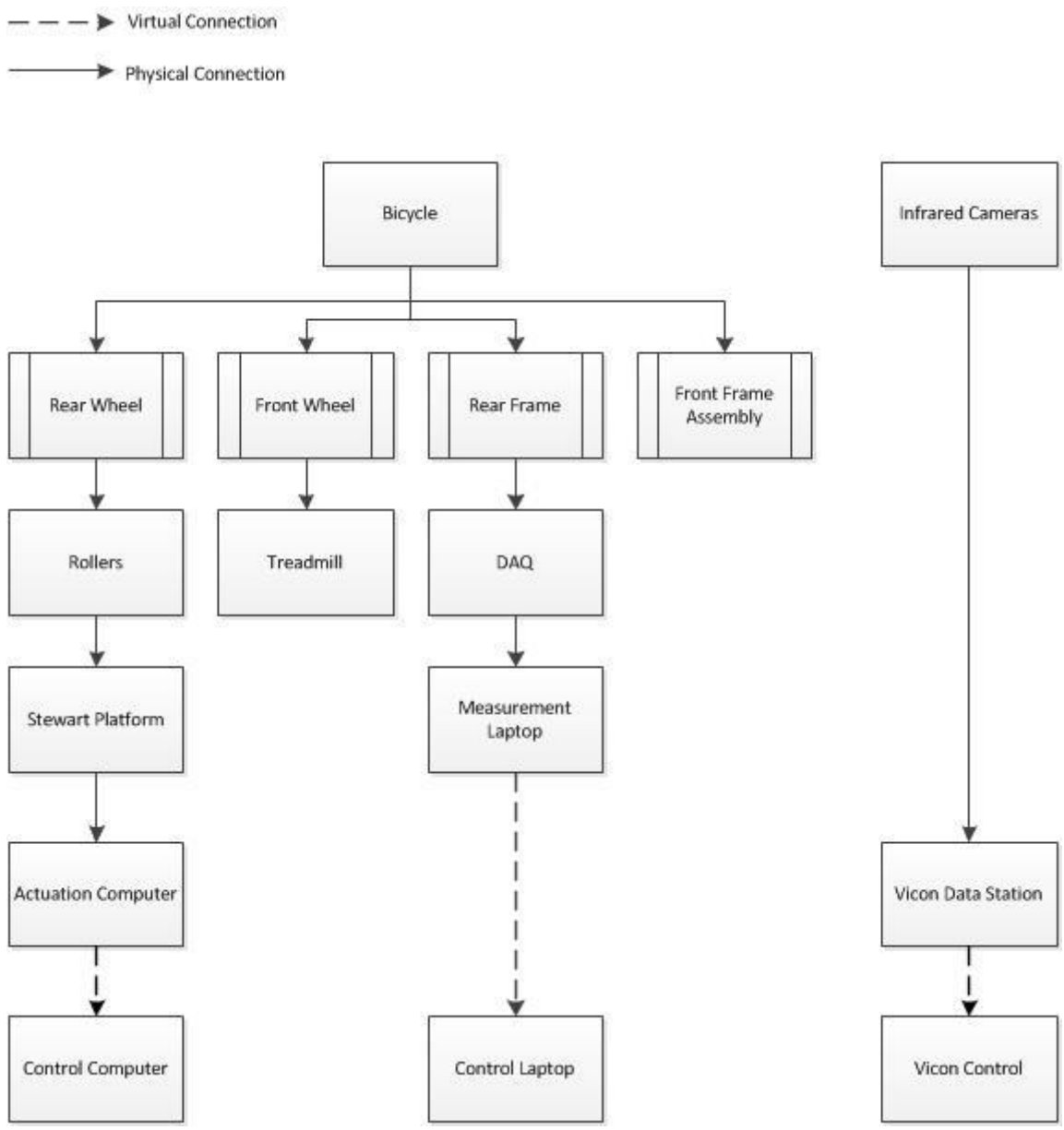

Appendix C – System of Systems of the Data Acquisition Card

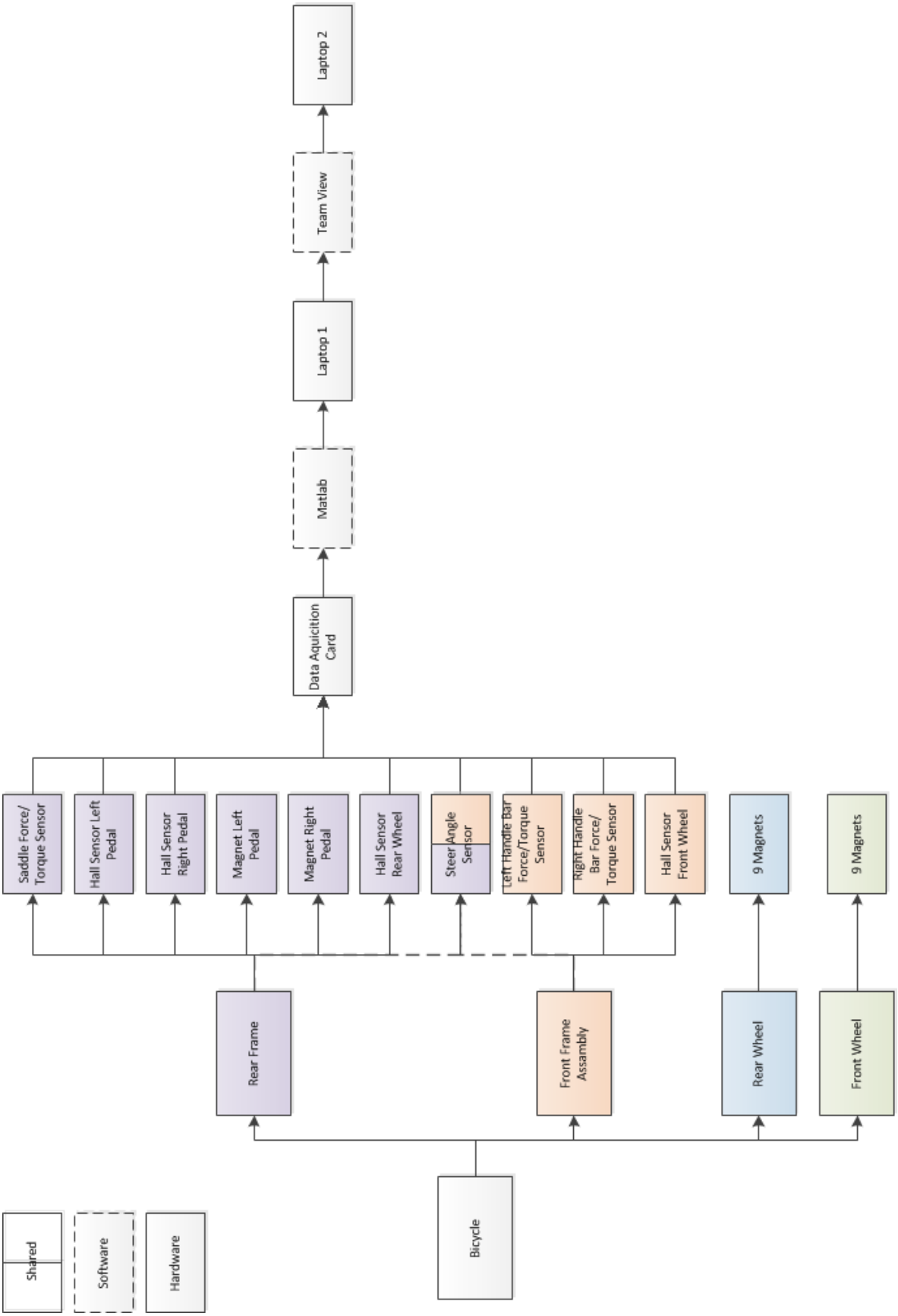

Appendix D – System of Systems of Vicon and the Stewart Platform

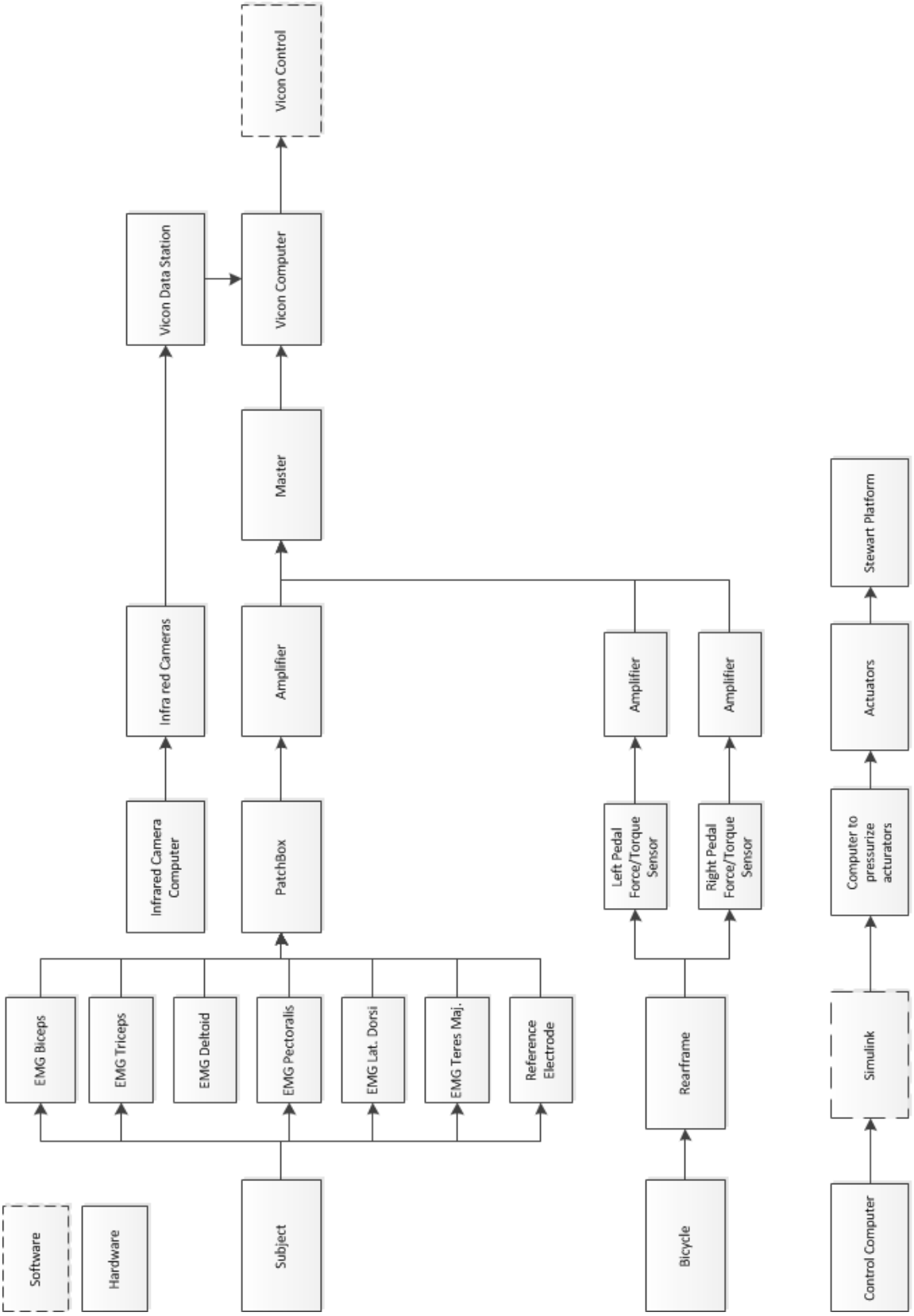

Appendix E – Bicycle Parameters

Segment	Variable	Value	STD	Dimension
Inertia front wheel	I_{FWxx}	0,122	0,013	[kg.m^2]
Inertia front wheel	I_{FWzz}	0,122	0,013	[kg.m^2]
Inertia front wheel	I_{FWy}	0,256	0,004	[kg.m^2]
Inertia rear wheel	I_{RWxx}	0,107	0,001	[kg.m^2]
Inertia rear wheel	I_{RWzz}	0,107	0,002	[kg.m^2]
Inertia rear wheel	I_{RWy}	0,268	0,008	[kg.m^2]
Inertia front frame	I_{FFxx}	0,272	0,002	[kg.m^2]
inertia front frame	I_{FFxz}	-0.146	0,002	[kg.m^2]
Inertia front frame	I_{FFzz}	0.178	0,003	[kg.m^2]
Inertia front frame	I_{FFy}	0,214	0,002	[kg.m^2]
Inertia rear frame	I_{RFxx}	0,469	0,027	[kg.m^2]
Inertia rear frame	I_{RFxz}	0,128	0,020	[kg.m^2]
Inertia rear frame	I_{RFzz}	0,610	0,018	[kg.m^2]
Inertia rear frame	I_{RFy}	1,105	0,021	[kg.m^2]
Mass front wheel	M_{FW}	3,720	0,020	[kg]
Mass rear wheel	M_{RW}	4,220	0,020	[kg]
Mass front frame	M_{FF}	3,720	0,020	[kg]
Mass rear frame	M_{RF}	8,620	0,020	[kg]
Radius front wheel	R_{FW}	0,355	-	[m]
Radius rear wheel	R_{RW}	0,356	-	[m]
Caster angle	λ	67,807	-	[degrees]
Wheel base	wb	1,125	-	[m]
Fork Offset	F_o	0,029	-	[m]
Trail	c	0,113	-	[m]
x CoM front wheel	x_{FW}	1,125	-	[m]
z CoM front wheel	z_{FW}	-0,355	-	[m]
x CoM rear wheel	x_{RW}	0,000	-	[m]
z CoM rear wheel	z_{RW}	-0,356	-	[m]
x CoM front frame	x_{FF}	0,907	0.0053	[m]
z CoM front frame	z_{FF}	-0,808	0.0031	[m]
x CoM rear frame	x_{RF}	0,334	0.0341	[m]
z CoM rear frame	z_{RF}	-0,466	0.0326	[m]
x CoM Bicycle	x_{RF}	0,515	-	[m]
z CoM Bicycle	z_{RF}	-0,486	-	[m]

Appendix F – Risk Analysis

Risk Factor	Critical Event	Effect	M	Frequency	Severness	RF
Wrong instruction to subject	deviating from protocol	increased risk for accidents	1, 18, 23	1	2	2
Inattentiveness			1, 18	1	2	2
Too strong perturbation	instbaility patient		3, 4 t/m 10	2	3	6
Insecurity subject			3, 4 t/m 11, 18, 19	2	3	6
Too difficult for subject			3, 4 t/m 12, 19	2	3	6
Steering error subject			4 t/m 11	2	3	6
Fatiguing subject			3, 4 t/m 11, 18, 22	2	3	6
Damaged sensor	malfunctiong sensor	Useless/Incorrect Data	13	2	2	4
Unsufficient periodical upkeep			13	1	1	1
Empty batteries			11, 12, 15, 16, 23	4	1	4
Sensor not switched on			16, 23	2	1	2
No/wrong synchronization	incorrect measured values		1	1	1	1
Empty batteries			11, 12, 15, 16, 23	4	1	4
Incorrect settings equipment			1, 14, 16, 23	2	1	2
No/Wrong calibration			1, 14, 123	1	1	1
excluding Subject	cancellation/delay measurement		1,3, 23	1	1	1
Malfunctioning equipment			13	2	1	2
Injury subject			1, 3, 4 t/m 11, 18, 19, 22	1	5	5
Deviation protocol	wrong velocity front and rear wheel		1	1	1	1
Multi Motor -and cognitive tasks subject			3, 17	2	1	2
Wrong perturbation parameters	Non-effectiveness Perturbation		1, 3	1	1	1
No/Wrong calibration	Noise motion system		1, 14	1	1	1
Reflecting artifacts			14, 25	2	1	2
Cable around pedal crank	Pedal FT-sensor cable breakage		18	1	2	2

Cable between treadmill			18	1	2	2
Subjects steps on cable			18	1	2	2
Subjects transpires	Sensor disengages	Useless Data	22	2	1	2
Insufficient skin contact			20, 21	1	1	1
Too long measurements			22	1	1	1
Programming error	Incorrect processing method	Incorrect Results	1, 2, 24	1	1	1
Incorrect Data storage			1, 2, 25	1	1	1

Appendix G– A3 information sheet contact forces

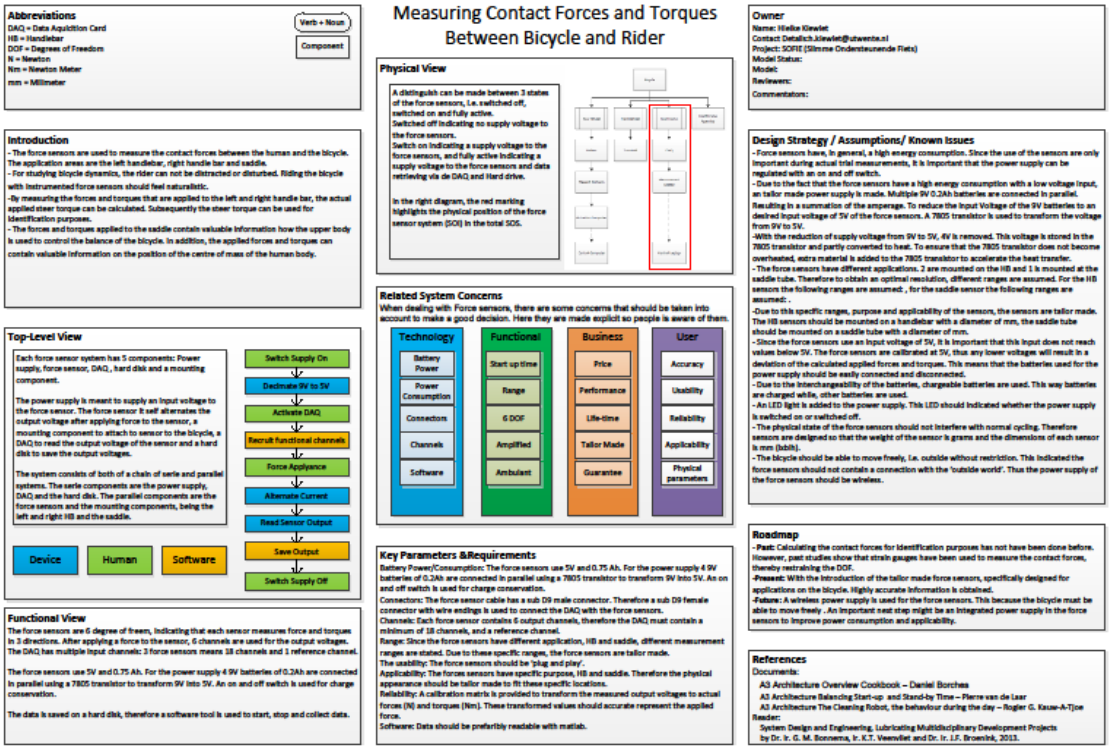

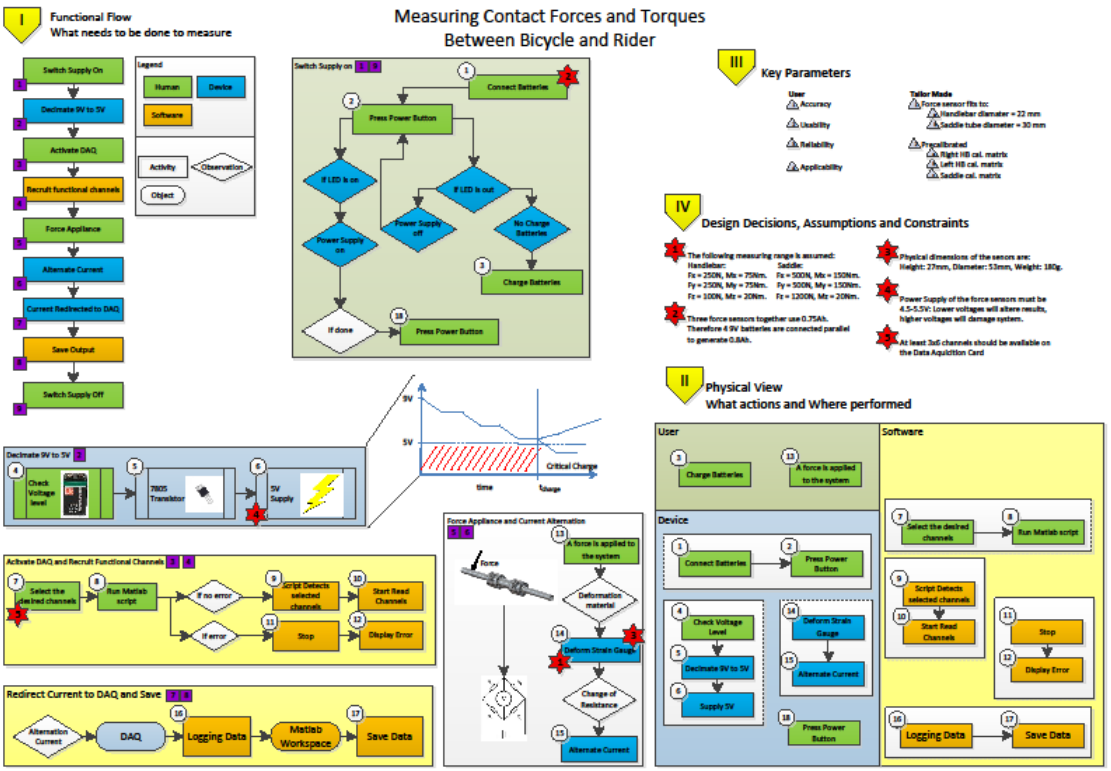

Appendix H – Medical Ethical Committee Approval

MEDISCH ETHISCHE TOETSINGSCOMMISSIE (METC)
TWENTE

Roessingh

Secretariaat METC, Medical School Twente, Institute voor Toegepast Wetenschappelijk Onderzoek,
Postbus 50.000, 7500 KA Enschede. Telefoon +31(0)53 487 [illegible] Fax +31(0)53 487 7047 Email: metc@mst.nl
Mw. ir. S.E.A. Sulink, arbeidelijk secretaris, telefoon +31(0)53 487 [illegible]

Roessingh Research and Development
T.a.v. Mw. R. Dubbeldam, MSc, PT, PhD
Postbus 310
7500 AH ENSCHEDE

Kenmerk: METC/14104.dub

Enschede, 25-03-2014

Betreft: **nader oordeel monocenterstudie, P12-31**, NL42027.044.12, ABR versie 07, definitief, 11 02-2014, protocol versie 4.0 d.d. 20-03-2014, SOFIE 12-31
Analysis of elderly cycling behaviour, fall risk and the relationship with physical and cognitive abilities. Protocol ID: SOFIE fietsgedrag van ouderen

Geachte mevrouw Dubbeldam,

Besluit
De Medisch Ethische ToetsingsCommissie Twente, METC Twente heeft zich op grond van artikel 2, tweede lid, sub a van de *Wet medisch wetenschappelijk onderzoek met mensen* (WMO), beraden over het amendement behorend bij, bovengenoemd onderzoeksdossier en over het toevoegen van een nieuw deelnemend centrum aan bovengenoemd onderzoek.
De commissie oordeelt <u>positief</u> over de toevoeging van deelnemend centrum:

- Universiteit Twente, Laboratory of Biomechanical Engineering te Enschede, mw. ir. V.E. Buisink

Het onderzoek was reeds goedgekeurd voor de volgende centra:

- Revalidatiecentrum Het Roessingh te Enschede, mw. R. Dubbeldam, PT;

De commissie oordeelt <u>positief</u> over het amendement.

Documenten
Het besluit is gebaseerd op de documenten die in bijlage 1 zijn vermeld.

Achtergrond
Op 20-02-2014 is het amendement ter beoordeling bij de METC Twente ingediend. Het amendement heeft betrekking op wijziging van het protocol en de toevoeging van Universiteit Twente als deelnemend centrum.

Het amendement is behandeld door het dagelijks bestuur in haar vergadering van 25-02-2014.

Overwegingen
De METC Twente is van oordeel dat aan alle voorwaarden in artikel 3 van de WMO is voldaan. De belangrijkste vragen waren over de uitbreiding van het protocol met een tweede fietstest, en speciaal de veiligheid van de daarbij gebruikte apparatuur en het veiligheidsharnas. De elektrische veiligheid is akkoord bevonden, dit geldt ook voor alle sensoren en andere apparatuur die bij het onderzoek verbonden worden met de proefpersoon. Nadere informatie van het veiligheidsharnas heeft geleerd dat het harnas een aan een vest verbonden draagconstructie betreft die opgehangen is aan het plafond. Dit is akkoord bevonden.

De commissie heeft de in bijlage 1 vermelde onderzoeksverklaring bekeken. Zij heeft geconstateerd dat is voldaan aan de voorwaarden in artikel 3, onderdeel e en j, van de WMO.

Appendix I – Scientific Publications, Proceedings and Presentations

Scientific Publications

2016
Kiewiet, H., Bulsink, V.E., Beugels, F., Koopman, H.F.J.M. The co-contraction index of the upper limb for young and old adult cyclists (2016) Accident Analysis and Prevention, . Article in Press.
DOI: 10.1016/j.aap.2016.04.036

2016
Vera E. Bulsink, Hielke Kiewiet, Dorien van de Belt, G. Maarten Bonnema, Bart Koopman, Cycling strategies of young and older cyclists, Human Movement Science, Volume 46, April 2016, Pages 184-195, ISSN 0167-9457, http://dx.doi.org/10.1016/j.humov.2016.01.005.

Proceedings

2015
Kiewiet H. , Bulsink V.E. , Beugels F. , Koopman H.F.J.M. . The Co-contract ion Index of the Upper Limb for Young and Old Adult Cyclists. International Cycling Safety Conference (ICSC), 15-16 September 2015, Hannover , Germany

2014
Kiewiet H., Bulsink V.E., van de Bel t D., Koopman H.F.J.M. A novel experimental setup to apply controlled disturbances to bicycle dynamics in a safe environment. International Design & Engineering Technical Conferences (ASME) , 17-20 Augustus 2014, Buffalo (NY) ,United States.

Presentations

2015
Kiewiet H. , Bulsink V.E. , Beugels F. , Koopman H.F.J.M. . The Co-contract ion Index of the Upper Limb for Young and Old Adult Cyclists. International Cycling Safety Conference (ICSC), 15-16 September 2015, Hannover , Germany

2014
Kiewiet H., Bulsink V.E., van de Bel t D., Koopman H.F.J.M. A novel experimental setup to apply controlled disturbances to bicycle dynamics in a safe environment. International Design & Engineering Technical Conferences (ASME) , 17-20 Augustus 2014, Buffalo (NY) ,United States.